学位論文

System Identification of Different Time-Scale Biological Phenomenon from Signal Transduction to Gene Expression

（シグナル伝達から遺伝子発現にかけて
異なる時間スケールで変動する
生命現象のシステム同定）

平成 29 年 12 月　博士（理学）申請

東京大学大学院理学系研究科
生物科学専攻
土屋　貴穂

Abstract

In intracellular signaling system, information of an extracellular stimulus is once encoded into combinations of distinct temporal patterns of phosphorylation of intracellular signaling at a scale of tens of minutes that are selectively decoded by downstream gene expression with a scale of hours to days, leading to cell fate decisions such as cell differentiation, proliferation and death (Behar and Hoffmann, 2010; Purvis and Lahav, 2013). In rat adrenal pheochromocytoma PC12 cells focused on in this study, nerve growth factor (NGF) induces cell differentiation mainly through sustained phosphorylation of ERK (Gotoh et al., 1990; Marshall, 1995; Qiu and Green, 1992; Traverse et al., 1992), whereas pituitary adenylate cyclase-activating polypeptide (PACAP) induces cell differentiation mainly through cAMP-dependent CREB phosphorylation (Akimoto et al., 2013; Gerdin and Eiden,11 2007; Saito et al., 2013; Vaudry et al., 2002; Watanabe et al., 2012), indicating that combinations of distinct temporal patterns of phosphorylation of intracellular signaling induce cell differentiation in PC12 cells (Vaudry et al., 2002).

In PC12 cell differentiation, key genes are also identified as the downstream decoding genes essential for cell differentiation in PC12 cells, including *Metrnl*, *Dclk1*, and *Serpinb1a*, denoted as LP (latent process) genes, which are the decoders of neurite length information (Watanabe et al., 2012). Importantly, the expression levels of the LP genes, but not the phosphorylation level of ERK, correlate with neurite length regardless of types of extracellular stimuli. Thus, this unrevealed decoding mechanism of signaling (a shorter time scale) dependent LP gene expression (a longer time scale) is a key issue for understanding the mechanism of cell differentiation. Thus, I focused on this decoding mechanism in this study.

To identify decoding mechanisms by gene expression, the system identification method was employed for identifying input–output relationships from time series data without detailed prior knowledge of signaling pathways (Janes and Lauffenburger, 2006; Janes and Yaffe, 2006; Kholodenko et al., 2012; Ljung, 2010; Price and Shmulevich, 2007; Zechner et al., 2016). In the previous study, a system identification method based on time series data of signaling molecules and gene expression, denoted as the nonlinear autoregressive exogenous

(NARX) model has been developed and applied it to the signaling-dependent immediate early genes (IEGs) expression during cell differentiation in PC12 cells (Saito et al., 2013). However, one of the difficulties of the NARX model is to require equally spaced dense time series data ideally. If the time scale of upstream and downstream molecules is different, such as signaling molecules (tens of minutes scale) and LP gene expression (a day scale) in this study (Doupé and Perrimon, 2014), it is technically difficult to obtain sufficient equally spaced dense time series data over the desirable time period due to experimental and budget limitations. Therefore, in reality, for a longer time scale experiment, unequally spaced sparse time series data rather than equally spaced dense time series data are available especially in biological experiments. However, no system identification method based on such sparse data due to different time scale exists.

Here I developed a system identification method by integrating the NARX model and a signal recovery technique in the field of compressed sensing originally developed for image analysis to biological sparse data of different time scales by recovering signals of missing time points (Summary Figure). I measured phosphorylation of ERK and CREB, IEGs expression products, and mRNAs of the decoder genes for neurite length in PC12 cell differentiation and performed the developed system identification, revealing the input–output relationships between signaling and gene expression with sensitivity such as graded or switch-like response and with time constant and gain, representing signal transfer efficiency (Summary Figure). Furthermore, I predicted and validated the identified system using pharmacological perturbation. The identifeid system was also princially consistent with the previous study (Saito et al., 2013).

I found that the LP genes depend only on the IEGs (c-Fos, FosB and/or JunB) but not other upstream molecules, and that the time constants of the LP genes are short except for *Serpinb1a*. This means that the timing of the final decoding step for neurite length information is not directly determined by the IEGs and LP genes, rather by the steps from extracellular stimuli to the IEGs. Furthermore, the identified system captured a selective NGF- and PACAP-signaling decoding system of neurite length information by LP gene

expression by using different signaling pathways.

The developed system identification method in this study can solve different time-scale problem and can be broadly applied to different time scale biological phenomena, such as the cell cycle, development, regeneration, and metabolism involving ion flux, metabolites, and gene expression not limited to this study case. Thus, I provide a versatile method for system identification of various biological phenomena using data with different time scales.

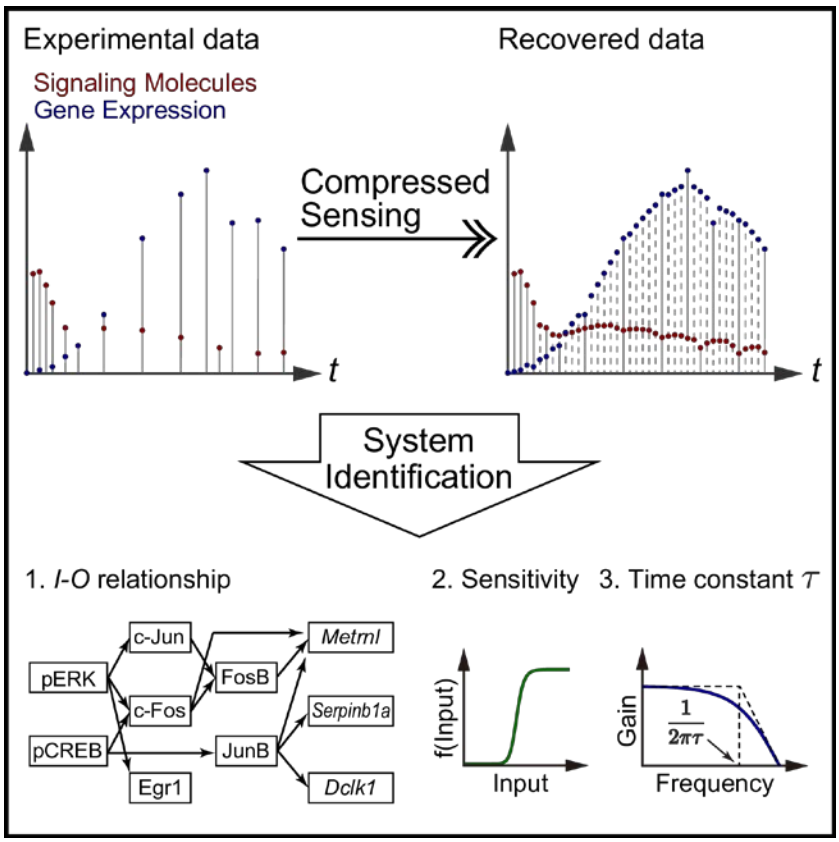

Summary figure. Schematic overview of system identification of different time-scale biological phenomenon.

Table of Contents

1. Introduction

1.1 Cell fate decisions by temporal coding in PC12 cell differentiation

In intracellular signaling systems, information of an extracellular stimulus is once encoded into combinations of distinct temporal patterns of phosphorylation of intracellular signaling molecules that are selectively decoded by downstream gene expression, leading to cell fate decisions such as cell differentiation, proliferation and death (Behar and Hoffmann, 2010; Purvis and Lahav, 2013). For instance, in rat adrenal pheochromocytoma PC12 cells, it has been reported that epidermal growth factor (EGF) induces cell proliferation thorough transient phosphorylation of ERK, whereas nerve growth factor (NGF) induces cell differentiation through sustained phosphorylation of ERK (Gotoh et al., 1990; Marshall, 1995; Qiu and Green, 1992; Traverse et al., 1992) (Figure 1). This phenomenon can be regarded that information of extracellular stimuli is once encoded into temporal patterns of ERK phosphorylation and decoded into each cell fate decision.

Furthermore, focusing on cell differentiation in PC12 cells, pituitary adenylate cyclase-activating polypeptide (PACAP) induces cell differentiation mainly through cAMP-dependent CREB phosphorylation rather than ERK phosphorylation (Akimoto et al., 2013; Gerdin and Eiden, 2007; Saito et al., 2013; Vaudry et al., 2002; Watanabe et al., 2012). In this PC12 cells differentiation by NGF or PACAP, it was shown that cell differentiation in PC12 cells can be divided into two processes: a latent processes (0–12 h after the stimulation) in preparation for neurite extension and a subsequent neurite extension process (12–24 h) (Chung et al., 2010; Watanabe et al., 2012). It was also indicated that latent process is dependent on ERK

phosphorylation and gene expression (Chung et al., 2010; Watanabe et al., 2012). In addition to that, Watanabe et al. identified the three genes essential for cell differentiation, *Metrnl*, *Dclk1*, and *Serpinb1a*, which are induced during the latent process and required for subsequent neurite extension, and named LP (latent process) genes (Watanabe et al., 2012). Although NGF and PACAP selectively induce the different combinations and temporal patterns of signaling molecules, both growth factors commonly induce the LP genes (Watanabe et al., 2012). The expression levels of LP genes, but not the phosphorylation level of ERK, correlate with neurite length regardless of growth factors (Watanabe et al., 2012), indicating that the LP genes are the decoders of neurite length and close to the phenotype (Figure 2). Since these key genes have been identified in cell differentiation in PC12 cells, I focused on how the distinct patterns of signaling molecules are decoded by LP gene expression which is critical for understanding the unrevealed mechanism underlying cell differentiation in PC12 cells.

Decoding the combinations and temporal patterns of signaling molecules by downstream gene expression is a quantitative mechanism generally involved in various cellular functions (Behar and Hoffmann, 2010; Purvis and Lahav, 2013; Sumit et al., 2017). In this PC12 cells case, Saito et al. previously revealed the decoding mechanism of signaling-dependent immediate early genes (IEGs) expression which are considered to be upstream of LP genes (Saito et al., 2013). Therefore, the research question in this study is to clarify the decoding mechanism of LP genes via ERK, CREB and IEGs (Figure 3).

1.2 Effectiveness and limitations of system identification method due to time-scale difference

Mathematical modeling is useful for the quantitative analysis of decoding mechanisms (Janes and Lauffenburger, 2013). If the signaling pathways are well characterized, kinetic modeling such as Ordinary Differential Equation (ODE) model based on biochemical reactions using information of the literature as prior knowledge is often employed (Janes and Lauffenburger, 2006; Kholodenko et al., 2012; Price and Shmulevich, 2007). For example, growth factor–dependent ERK activation in PC12 cells has been modeled by the kinetic model based on prior knowledge of pathway information (Brightman and Fell, 2000; Filippi et al., 2016; Nakakuki et al., 2010; Ryu et al., 2015; Santos et al., 2007; Sasagawa et al., 2005). In general, however, decoding by downstream genes involves more complex processes such as transcription and translation and information on the precise pathway is not available.

To identify decoding mechanisms by gene expression, the system identification method (also referred to as data-driven modeling) was employed for identifying input–output relationships from time series data without detailed prior knowledge of signaling pathways (Janes and Lauffenburger, 2006; Janes and Yaffe, 2006; Kholodenko et al., 2012; Ljung, 2010; Price and Shmulevich, 2007; Zechner et al., 2016). In the previous study, a system identification method based on time series data of signaling molecules and gene expression, denoted as the nonlinear autoregressive exogenous (NARX) model has been developed and applied it to the signaling-dependent IEGs expression during cell differentiation in PC12 cells (Saito et al., 2013). The NARX model involves the determination of lag-order numbers and use of the Hill equation and the linear autoregressive exogenous (ARX) model (Saito et al.,

2013). Determination of lag-order numbers infers the selection of input molecules (*Input*) for an output molecule (*Output)*, which is referred to as the *Input-Output* (*I-O*). The Hill equation characterizes sensitivity with a nonlinear dose-response curve (Hill, 1910). The linear ARX model characterizes temporal changes with time constant and gain, the latter of which is an *I-O* amplitude ratio, and indicates signal transfer efficiency (Ljung, 1998). The advantages of the NARX model rather than kinetic model is systematically presentation of model candidates without detailed prior knowledge of signaling pathway. However, one of the difficulties of the NARX model is to require equally spaced dense time series data ideally. If the time scale between upstream and downstream are similar, such as signaling molecules (tens of minutes scale) and IEGs expression (a few hours scale) in PC12 cells, it is not difficult to acquire a sufficient number of equally spaced dense time series data (Saito et al., 2013). However, if the time scale of upstream and downstream molecules is different, such as signaling molecules (tens of minutes scale) and LP gene expression (a day scale) (Doupé and Perrimon, 2014), it is technically difficult to obtain sufficient equally spaced dense time series data over the desirable time period due to experimental and budget limitations.

Measuring gene expression often requires a longer time scale than measuring protein phosphorylation. Obtaining equally spaced dense time series data with a longer time scale takes labor and intensive cost, because, unlike live-cell imaging experiments, snapshot experiments such as western blotting, RT-PCR, and quantitative image cytometry (QIC) which is one of the quantitative fluorescence immuno-staining techniques (Ozaki et al., 2010) require the number of experiments proportional to the number of time points. In addition to

that, experimental noise and variation increases as the number of experiments increases because differences in experimental conditions occur such as difference of plates, gels, reagents, and cell culture conditions across the experiments. Therefore, in reality, for a longer time scale experiment, unequally spaced sparse time series data rather than equally spaced dense time series data are available especially in biological experiments. For example, under conditions in which stimulation by cell growth factors triggers rapid and transient phosphorylation and slow and sustained gene expression, time series data should be obtained with dense time points during the transient phase and eventually with sparse time points in reality. The timing and dynamic characteristics of temporal changes may differ between upstream and downstream molecules, such that time points and intervals for measuring upstream and downstream molecules may be different. Thus, in order to clarify the decoding mechanism of different time scale biological phenomenon, a system identification method using unequally spaced sparse time series data with different time scale needs to be developed.

Unequally spaced sparse time series data can be regarded as equally spaced dense time series data with missing time points, and therefore equally spaced dense time series data can be generated by applying a signal recovery technique, which has been studied in the field of compressed sensing (Candès and Wakin, 2008; Donoho, 2006). Compressed sensing is a signal processing method for efficient data acquisition by recovering missing signals/images from a small number of randomly sampled signals including unequally spaced sparse data based on sparseness of a vector (Candès et al., 2008) or low rankness of a matrix (Fazel,

2002). Both the sparse approach and the low-rank approach have been applied to various fields, such as sampling and reconstructing magnetic resonance images (Lustig et al., 2008; Ongie and Jacob, 2016), super-resolution imaging (Candès and Fernandez-Granda, 2014; Yang et al., 2010), image inpainting (Takahashi et al., 2012; Takahashi et al., 2016), and collaborative filtering (Candès and Recht, 2009). In this study, I applied a matrix rank minimization algorithm (Konishi et al., 2014) to recover missing time points from unequally spaced time series data, and generated equally spaced time series data with the same time points from signaling and gene expression data with different time scales. A system identification method from equally spaced dense time series data of signaling and gene expression employing the NARX model has been previously developed (Saito et al., 2013). In this study, I developed a new system identification method from unequally spaced sparse time series data with different time scales by integrating this signal recovery method employing the matrix rank minimization algorithm (Konishi et al., 2014) and the NARX model (Saito et al., 2013).

1.3 Purpose of this study

Thus, to summarize these above points, the purposes in this study are to develop a system identification method using unequally spaced sparse time series data with different time scale and to clarify the decoding mechanism of LP genes via ERK, CREB and IEGs employing the developed system identification method. To solve the former problem due to different time scale data, here I applied the signal recovery technique based on the low-rank

approach in the field of compressed sensing to recover a sufficient number of time points for equally spaced dense time series data from unequally spaced sparse time series data with different time points and intervals. Then, to solve the latter problem, I applied this system identification method to the signaling and IEGs dependent LP genes expression underlying cell differentiation in PC12 cells and identified the signaling-decoding system by LP genes expression.

2. Materials and methods

2.1 Cell culture and treatments

Culture of PC12 cells by growth factors (Saito et al., 2013) was performed as previously described. Briefly, PC12 cells (kindly provided by Masato Nakafuku, Cincinnati Children's Hospital Medical Center, Cincinnati, OH, USA) (Sasagawa et al., 2005) were cultured at 37°C under 5% CO_2 in complete medium, Dulbecco's modified Eagle's medium (DMEM) (Sigma, Zwijndrecht, The Netherlands) supplemented with 10% fetal bovine serum (Sigma) and 5% horse serum (Gibco, Bethesda, MD, USA). For stimulation, PC12 cells were plated on poly-L-lysine-coated 96-well microplates (0.5×10^4 cells/well) in the complete medium for 24 h and then treated with the complete medium in the presence or absence of the indicated doses of NGF (R&D Systems, Minneapolis, MN, USA), PACAP (Sigma), and PMA (Sigma) (Saito et al., 2013; Uda et al., 2013). Stimulations for cells seeded in 96-well microplates were performed by using a liquid handling system (Biomek NX Span-8, Beckman Coulter, Fullerton, CA, USA) with an integrated heater-shaker (Variomag, Daytona Beach, FL, USA) and robotic incubator (STX-40, Liconic, Mauren, Liechtenstein). For the inhibitor experiment, I stimulated cells with PACAP in the presence of 10 μM trametinib (Selleckchem, Houston, TX, USA). The inhibitor was added 30 min before stimulation with PACAP.

2.2 Quantitative image cytometry

QIC was performed as previously described (Ozaki et al., 2010). Briefly, after

stimulation by the growth factors, the cells were fixed, washed with phosphate-buffered saline, and permeabilized with blocking buffer (0.1% Triton X-100, 10% fetal bovine serum in phosphate-buffered saline). The cells were washed and then incubated for 2 h with primary antibodies diluted in Can Get Signal immunostain Solution A (Toyobo, Osaka, Japan). The cells were washed three times and then incubated for 1 h with second antibodies. After immunostaining, the cells were stained for the nucleus by incubating with Hoechst 33342 (Invitrogen, Carlsbad, CA, CA). The images of the stained cells were acquired by using a CellInsite NTX (Thermo Fisher Scientific) automated microscope with a 20× objective lens. For QIC analyses, I acquired different field images of the cells in each well, until the number of obtained cells exceeded 1000. Liquid handling for the 96-well microplates was performed using a Biomek NX Span-8 liquid handling system. Intensities of the signaling activity and the Immediate Early Genes (IEGs) between experiments were normalized by an internal control of each 96-well plate in QIC. Note that for the QIC assays, all the cells within a plate were fixed simultaneously to prevent the exposure of cells to formaldehyde vapor during the treatment.

2.3 qRT-PCR analysis

Reverse transcription–polymerase chain reaction (RT-PCR) was performed as previously described (Watanabe et al., 2012). Briefly, total RNA was prepared from PC12 cells using an Agencourt RNAdvance Tissue Kit according to the manufacturer’s instructions (Beckman Coulter, La Brea, CA, USA). RNA samples were reverse transcribed by using a High

Capacity RNA-to-cDNA Kit (Applied Biosystems, Carlsbad, CA, USA) and the resulting cDNAs were used as templates for qRT-PCR. qRT-PCR was performed with Power SYBR Green PCR Master Mix (Applied Biosystems) and the primers are shown in Table 1. As an internal control for normalization, the β-actin transcript was similarly amplified using the primers. qRT-PCR was conducted using a 7300 Real Time PCR System (Applied Biosystems), and the data were acquired and analyzed by the 7300 System SDS software version 1.3.1.21 (Applied Biosystems).

2.4 NARX model and data representation

In this study, assuming that the input molecules (*Input*) and output molecules (*Output*) signals satisfy the following NARX model, Eqs (1) and (2), the system identification is performed by estimating unknown parameters in the NARX model,

$$y_k^{p,s} = \sum_{i=1}^{m_y} a_i^p \, y_{k-i}^{p,s} + \sum_{q \in \mathcal{M}_p} \sum_{j=1}^{m_u} b_j^p f(u_{k-j}^{q,s}, n_p, K_p), \tag{1}$$

$$f(u, n, K) = \frac{u^n}{u^n + K^n}, \tag{2}$$

where $u_k^{q,s}$ and $y_k^{p,s}$ are experimental values of *Input* and *Output* at time step k, p and q respectively denote indices of *Output* and *Input* defined in the following sets in this study,

$$p \in P = \{\text{c-Jun}, \text{Egr1}, \text{c-Fos}, \text{FosB}, \text{JunB}, Metrnl, Serpinb1a, Dclk1\text{A}\}, \tag{3}$$

$$q \in \mathcal{M}_p \subseteq \mathcal{M} = \{\text{pERK}, \text{pCREB}, \text{c-Jun}, \text{Egr1}, \text{c-Fos}, \text{FosB}, \text{JunB}\}, \tag{4}$$

and s is an index of stimulation conditions of the experiments defined as follows in this study,

$$s \in \{\mathrm{NGF}, \mathrm{PACAP}, \mathrm{PMA}\}. \quad (5)$$

$\mathcal{M}_p$ is the index set of *Input* defined for each *Output* $p \in P$ as described in Results. The nonlinear function $f(x)$ in Eq (2) is the Hill equation that describes a sigmoidal curve based on biochemical reaction and is widely used in the field of biology (Hill, 1910). The coefficients a_i^p and b_j^p, the orders m_y and m_u in Eq (1), n_p and K_p in Eq (2), and set $\mathcal{M}_p$ are unknown parameters. For each molecule under stimulation condition s (NGF, PACAP, and PMA), the unequally spaced time series data are obtained by the experiments in this study. These data can be considered as equally spaced time data $u_k^{q,s}$ and $y_k^{p,s}$ with missing time points and the unknown NARX parameters can be estimated after recovering missing time points based on the low rankness of the Hankel-like matrix, which is described in the next section "Extension of ARX system identification from unequally spaced time series data to the nonlinear ARX system".

2.5 Extension of ARX system identification from unequally spaced time series data to the nonlinear ARX system

To handle the nonlinear ARX system, I extended ARX system identification from unequally spaced time series data to the nonlinear ARX system. First, I consider and formulate the simple case of the linear ARX model and then extend it to the NARX model. To carry out system identification from unequally spaced time series data, equally spaced time series data need to be generated by signal recovery of missing time points. In the case that the *Input* and *Output* data of a linear system are missing and the order of the system is unknown as in this study, the system identification using the recovered *Input* and *Output* data

based on the low rankness of the Hankel-like matrix has been proposed and applicable (Liu et al., 2013). This method enables us to recover missing data by solving the matrix rank minimization problem and to generate equally spaced time series data for system identification. In this study, I apply this matrix rank minimization approach to simultaneously identify the NARX model and recover missing time points data.

For simplicity, let me consider the case of the linear ARX model with single *Input* and single *Output* described by

$$y_k = \sum_{i=1}^{m_y} a_i y_{k-i} + \sum_{j=1}^{m_u} b_j u_{k-j} + v_k, \tag{6}$$

where y_k and u_k are the *Output* and *Input* at time step k, and v_k is the noise. When only $\{u_k\}_{k\in\Omega_u}$ and $\{y_k\}_{k\in\Omega_y}$ are obtained, that is, the part of the *Input* and *Output* data $\{u_k\}_{k=1}^{N}$ and $\{y_k\}_{k=1}^{N}$, the problem can be considered as the recovery of unknown *Input* and *Output* data. Here, Ω_u and Ω_y are index sets and are a subset of the set $\{1,2,\dots,N\}$. Hankel-like matrices are defined as Y and U by Eqs (7) and (8), where it is assumed that N is sufficiently larger than r.

$$Y = \begin{bmatrix} y_1 & y_2 & y_3 & \cdots & y_r \\ y_2 & y_3 & y_4 & \cdots & y_{r+1} \\ y_3 & y_4 & y_5 & \cdots & y_{r+2} \\ \vdots & \vdots & \vdots & \ddots & \vdots \\ y_{N-r+1} & y_{N-r+2} & y_{N-r+3} & \cdots & y_N \end{bmatrix} \tag{7}$$

$$U = \begin{bmatrix} u_1 & u_2 & u_3 & \cdots & u_r \\ u_2 & u_3 & u_4 & \cdots & u_{r+1} \\ u_3 & u_4 & u_5 & \cdots & u_{r+2} \\ \vdots & \vdots & \vdots & \ddots & \vdots \\ u_{N-r+1} & u_{N-r+2} & u_{N-r+3} & \cdots & u_N \end{bmatrix}. \tag{8}$$

Hankel-like matrices Y and U are matrices called Hankel matrices if they are square matrices, and they are matrices in which the same components are entered from the lower left

to the upper right in the matrix. Considering $v_k = 0$ in Eq (6), that is, considering an ideal case without noise, Eq (9) holds for the matrix $[Y\ U]$ in which the matrices Y and U are arranged horizontally (Figure 4B).

$$\text{rank}[Y\ U] = \text{m}_\text{y} + r < 2r \tag{9}$$

Thus, the matrix $[Y\ U]$ is a low-rank matrix whose rank is determined by the order of the system. If m_y is known in Eq (9), the missing data can be recovered by restoring the unknown elements of the matrix so that the rank of the matrix $[Y\ U]$ becomes $m_y + r$. Because the order m_y is unknown in this study, the unknown elements are recovered so as to minimize the rank of the matrix $[Y\ U]$ based on the idea that it is better to describe the system with as few parameters as possible. That means the missing data are recovered by solving the matrix rank minimization problem in this study as follows,

$$\begin{gathered}\text{Minimize rank}[Y\ U] \\ \text{subject to } y_k = \bar{y}_k \text{ for all } k \in \Omega_y \\ u_k = \bar{u}_k \text{ for all } k \in \Omega_u,\end{gathered} \tag{10}$$

where $\bar{y}_k$ and $\bar{u}_k$ are observed values. Eq (10) is a nonconvex optimization problem, which is generally a Non-deterministic Polynomial time (NP)-hard problem in the field of the computational complexity theory. Therefore, I handle the relaxation problem of this problem in Eq (11) in which the objective function is replaced by the nucleus norm, the sum of the singular values of the matrix, and obtain a low-rank matrix by solving this optimization problem with the iterative partial matrix shrinkage (IPMS) algorithm (Konishi et al., 2014).

$$\begin{gathered}\text{Minimize } \|[Y\ U]\|_{*,r} \\ \text{subject to } y_k = \bar{y}_k \text{ for all } k \in \Omega_y \\ u_k = \bar{u}_k \text{ for all } k \in \Omega_u,\end{gathered} \tag{11}$$

where $\|\cdot\|_{*,r}$ represents the sum of singular values that are smaller than the *r*th greater

singular value. The IPMS algorithm is a technique to provide a low-rank solution of Eq (10) by solving Eq (11) repeatedly for increasing r by 1, starting at $r = 0$, and provides recovered data with small energy loss after recovery and less distortion of the original matrices by preferentially estimating from a singular value of a large value (Konishi et al., 2014).

In the case of a multi-*Input* system, for each *Input*, a Hankel-like matrix U_l corresponding to the matrix U is prepared, and by solving the matrix rank minimization problem of matrices arrayed side by side such as $[Y\ U_1 \ldots U_L]$, *Inputs* and *Output* data can be similarly recovered. Also, in the case that data under multiple stimulation conditions are obtained as in this study, *Input* and *Output* data can be recovered by arranging the matrices vertically for each stimulation condition. For example, when there is a data set of NGF stimulation and PACAP stimulation and simulation condition s is $s \in \{\mathrm{NGF}, \mathrm{PACAP}\}$, a matrix composed of y_k^s and u_k^s is vertically arranged for each stimulation condition s to construct Y and U, and *Input* and *Output* data can be recovered by solving the matrix rank minimization problem for $[Y\ U]$.

$$[Y] = \begin{bmatrix} y_1^{NGF} & y_2^{NGF} & y_3^{NGF} & \cdots & y_r^{NGF} \\ y_2^{NGF} & y_3^{NGF} & y_4^{NGF} & \cdots & y_{r+1}^{NGF} \\ y_3^{NGF} & y_4^{NGF} & y_5^{NGF} & \cdots & y_{r+2}^{NGF} \\ \vdots & \vdots & \vdots & \ddots & \vdots \\ y_{N-r+1}^{NGF} & y_{N-r+2}^{NGF} & y_{N-r+3}^{NGF} & \cdots & y_N^{NGF} \\ y_1^{PACAP} & y_2^{PACAP} & y_3^{PACAP} & \cdots & y_r^{PACAP} \\ y_2^{PACAP} & y_3^{PACAP} & y_4^{PACAP} & \cdots & y_{r+1}^{PACAP} \\ y_3^{PACAP} & y_4^{PACAP} & y_5^{PACAP} & \cdots & y_{r+2}^{PACAP} \\ \vdots & \vdots & \vdots & \ddots & \vdots \\ y_{N-r+1}^{PACAP} & y_{N-r+2}^{PACAP} & y_{N-r+3}^{PACAP} & \cdots & y_N^{PACAP} \end{bmatrix} \tag{12}$$

$$[U] = \begin{bmatrix} u_1^{NGF} & u_2^{NGF} & u_3^{NGF} & \cdots & u_r^{NGF} \\ u_2^{NGF} & u_3^{NGF} & u_4^{NGF} & \cdots & u_{r+1}^{NGF} \\ u_3^{NGF} & u_4^{NGF} & u_5^{NGF} & \cdots & u_{r+2}^{NGF} \\ \vdots & \vdots & \vdots & \ddots & \vdots \\ u_{N-r+1}^{NGF} & u_{N-r+2}^{NGF} & u_{N-r+3}^{NGF} & \cdots & u_N^{NGF} \\ u_1^{PACAP} & u_2^{PACAP} & u_3^{PACAP} & \cdots & u_r^{PACAP} \\ u_2^{PACAP} & u_3^{PACAP} & u_4^{PACAP} & \cdots & u_{r+1}^{PACAP} \\ u_3^{PACAP} & u_4^{PACAP} & u_5^{PACAP} & \cdots & u_{r+2}^{PACAP} \\ \vdots & \vdots & \vdots & \ddots & \vdots \\ u_{N-r+1}^{PACAP} & u_{N-r+2}^{PACAP} & u_{N-r+3}^{PACAP} & \cdots & u_N^{PACAP} \end{bmatrix} \quad (13)$$

In the NARX model employed in this study, because the observed *Input* data is nonlinearly transformed using the nonlinear function *f* in Eq (2) and the nonlinearly transformed *Input* data and the *Output* data follow the ARX system, signal recovery and system identification can be performed on the nonlinearly transformed *Input*, not but untransformed *Input* data, and *Output* data by the above method. Based on this idea, I performed nonlinear ARX system identification.

2.6 Procedure for system identification by integrating signal recovery and the NARX model

Note that this procedure corresponds to flowchart in Figure 6B. To estimate an *I-O* relationship, data sets of all combinations of input molecules (*Inputs*) for each output molecule (*Output*) are prepared. For each data set, leave-one-out cross-validation is performed by preparing all combinations with only one test data set and the rest as the training data set. Three stimulation conditions, NGF, PACAP, and PMA, are obtained and used two of them as the training data set and the other one as the test data set in this study. Therefore, there are three combinations to divide the test and training data sets.

In nonlinear systems such as the NARX model in this study, even if all the *Input* and *Output* data are known, obtaining n_p and K_p is a nonconvex optimization problem, for which it is difficult to obtain an exact solution. Therefore, n_p and K_p are estimated by 500 trials with multiple random initial values. By repeating the following procedures from step i to step v, n_p and K_p are estimated so as to minimize the AIC for the training data set, while *Inputs* and *Output* of the NARX model are recovered. Subsequently, signal recovery of the test data set is performed in step vi, and the residual sum of square (RSS) is calculated for a test data set in step vii. Step vii is performed with all three combinations of training and test data sets, and take the sum of RSS for test data sets. Step viii is performed with all combinations of *Input*, and then in step ix a combination of *Input* with the minimum sum of RSS for test data sets is selected. This combination of *Inputs* is used for the *I-O* relationship. Using the combination of the *Input* molecules in step x and the data set of all stimulation conditions as the training data set, I estimate the parameters of the NARX model, which is used as the finally obtained NARX model.

Step i: Nonlinear transformation of *Input* data by the Hill equation.

$u_k^{q,s}$, which is *Input* q at time step k under the stimulation condition s, is transformed into $x_k^{q,s} = f(u_k^{q,s})$ by Eq (2), the Hill equation. The initial values of n_p and $K_p^{n_p}$ are given by $n_p = 1$ and a uniform random number between 0 to 1, respectively, for each *Input q*. Using the observed *Output* $y_k^{p,s}$ and the nonlinearly transformed *Input* $x_k^{q,s}$, the following Hankel-

like matrix is constructed for *Output* p while assigning the previous closest observation value to the initial value of missing points. Note that this is a notation in the case of a single *Input*. Hereafter, two training data sets and one test data set are referred as $training\ 1$ and $training\ 2$ and $test$, respectively.

$$[Y] = \begin{bmatrix} y_1^{training\ 1} & y_2^{training\ 1} & y_3^{training\ 1} & \cdots & y_r^{training\ 1} \\ y_2^{training\ 1} & y_3^{training\ 1} & y_4^{training\ 1} & \cdots & y_{r+1}^{training\ 1} \\ y_3^{training\ 1} & y_4^{training\ 1} & y_5^{training\ 1} & \cdots & y_{r+2}^{training\ 1} \\ \vdots & \vdots & \vdots & \ddots & \vdots \\ y_{N-r+1}^{training\ 1} & y_{N-r+2}^{training\ 1} & y_{N-r+3}^{training\ 1} & \cdots & y_N^{training\ 1} \\ \\ y_1^{training\ 2} & y_2^{training\ 2} & y_3^{training\ 2} & \cdots & y_r^{training\ 2} \\ y_2^{training\ 2} & y_3^{training\ 2} & y_4^{training\ 2} & \cdots & y_{r+1}^{training\ 2} \\ y_3^{training\ 2} & y_4^{training\ 2} & y_5^{training\ 2} & \cdots & y_{r+2}^{training\ 2} \\ \vdots & \vdots & \vdots & \ddots & \vdots \\ y_{N-r+1}^{training\ 2} & y_{N-r+2}^{training\ 2} & y_{N-r+3}^{training\ 2} & \cdots & y_N^{training\ 2} \end{bmatrix} \tag{14}$$

$$[U] = \begin{bmatrix} x_1^{training\ 1} & x_2^{training\ 1} & x_3^{training\ 1} & \cdots & x_r^{training\ 1} \\ x_2^{training\ 1} & x_3^{training\ 1} & x_4^{training\ 1} & \cdots & x_{r+1}^{training\ 1} \\ x_3^{training\ 1} & x_4^{training\ 1} & x_5^{training\ 1} & \cdots & x_{r+2}^{training\ 1} \\ \vdots & \vdots & \vdots & \ddots & \vdots \\ x_{N-r+1}^{training\ 1} & x_{N-r+2}^{training\ 1} & x_{N-r+3}^{training\ 1} & \cdots & x_N^{training\ 1} \\ \\ x_1^{training\ 2} & x_2^{training\ 2} & x_3^{training\ 2} & \cdots & x_r^{training\ 2} \\ x_2^{training\ 2} & x_3^{training\ 2} & x_4^{training\ 2} & \cdots & x_{r+1}^{training\ 2} \\ x_3^{training\ 2} & x_4^{training\ 2} & x_5^{training\ 2} & \cdots & x_{r+2}^{training\ 2} \\ \vdots & \vdots & \vdots & \ddots & \vdots \\ x_{N-r+1}^{training\ 2} & x_{N-r+2}^{training\ 2} & x_{N-r+3}^{training\ 2} & \cdots & x_N^{training\ 2} \end{bmatrix} \tag{15}$$

Step ii: Signal recovery of training data.

Solve the matrix $[Y\ U]$ rank minimization problem of Eq (11) by the IPMS algorithm and recover converted *Input* data $x_k^{q,s}$ and *Output* data $y_k^{p,s}$. Note that, in the case of multi-*Input*, for each *Input*, a matrix U_l corresponding to the matrix U is generated, and by solving the

matrix rank minimization problem of matrices arrayed side by side such as $[Y\ U_1\ ...\ U_L]$, *Inputs* and *Output* data can be similarly recovered.

Step iii: Calculate ARX parameters, $\boldsymbol{a}$ and $\boldsymbol{b}$.

Based on the relationship between the Hankel-like matrix and ARX parameters (Figure 4B), obtain the ARX parameters a_i^p and b_j^p in Eq (1) for *Output* p and each *Input* q using the recovered transformed *Input* data $x_k^{q,s}$ and *Output* data $y_k^{p,s}$. The order of the system, the lag order of the ARX model, is determined based on the matrix rank obtained in step ii.

Step iv: Estimate n_p and $K_p^{n_p}$ using the recovered data and ARX parameters.

Using the inverse function *f* of Eq (2), recover the missing time point data of *Input* before transformation by using Eq (2). To reduce computational cost by repeating IPMS algorithm, the recovered $x_k^{q,s}$ and $y_k^{p,s}$ are reused in this step. For the recovered $x_k^{q,s}$ and $y_k^{p,s}$, n_p in Eq (2) is given again by uniform random numbers >1 and ≤100 and $K_p^{n_p}$ ≥0.001 and ≤1, and 200 combinations of n_p and $K_p^{n_p}$ are generated. For each combination, perform simulation of the ARX model and calculate AIC for the training data set, $AIC_{training}$. Select the combination of n_p and $K_p^{n_p}$ with the minimum $AIC_{training}$. Using this n_p and $K_p^{n_p}$, *Input* and *Output* data in the matrix $[Y\ U]$ composed of Y and U in Eqs (14) and (15) is recovered again by the IPMS algorithm. Note that during IPMS process, AIC not but RSS is used because numbers of lag order change due to the change of matrix rank.

Step v: Select NARX parameters with the minimum $AIC_{training}$.

Repeat steps i to iv 500 times. Select n_p and $K_p^{n_p}$ and ARX parameters that minimize $AIC_{training}$.

Step vi: Signal recovery of test data.

Using the n_p, $K_p^{n_p}$ and ARX parameters selected in step v, add test data to the recovered matrix $[Y\ U]$ in Eqs (14) and (15) like in Eqs (16) and (17). Test data are also recovered by solving the test data added matrix $[Y\ U]$ rank minimization problem with the IPMS algorithm. Note that training data sets have already been recovered until step v. Therefore, with the training data fixed, IPMS was applied to the matrix combining the test data, and signal recovery of only test data is performed in this step.

$$[Y] = \begin{bmatrix} y_1^{training\,1} & y_2^{training\,1} & y_3^{training\,1} & \cdots & y_r^{training\,1} \\ y_2^{training\,1} & y_3^{training\,1} & y_4^{training\,1} & \cdots & y_{r+1}^{training\,1} \\ y_3^{training\,1} & y_4^{training\,1} & y_5^{training\,1} & \cdots & y_{r+2}^{training\,1} \\ \vdots & \vdots & \vdots & \ddots & \vdots \\ y_{N-r+1}^{training\,1} & y_{N-r+2}^{training\,1} & y_{N-r+3}^{training\,1} & \cdots & y_N^{training\,1} \\ y_1^{training\,2} & y_2^{training\,2} & y_3^{training\,2} & \cdots & y_r^{training\,2} \\ y_2^{training\,2} & y_3^{training\,2} & y_4^{training\,2} & \cdots & y_{r+1}^{training\,2} \\ y_3^{training\,2} & y_4^{training\,2} & y_5^{training\,2} & \cdots & y_{r+2}^{training\,2} \\ \vdots & \vdots & \vdots & \ddots & \vdots \\ y_{N-r+1}^{training\,2} & y_{N-r+2}^{training\,2} & y_{N-r+3}^{training\,2} & \cdots & y_N^{training\,2} \\ y_1^{test} & y_2^{test} & y_3^{test} & \cdots & y_r^{test} \\ y_2^{test} & y_3^{test} & y_4^{test} & \cdots & y_{r+1}^{test} \\ y_3^{test} & y_4^{test} & y_5^{test} & \cdots & y_{r+2}^{test} \\ \vdots & \vdots & \vdots & \ddots & \vdots \\ y_{N-r+1}^{test} & y_{N-r+2}^{test} & y_{N-r+3}^{test} & \cdots & y_N^{test} \end{bmatrix} \quad (16)$$

$$[U] = \begin{bmatrix} x_1^{training\,1} & x_2^{training\,1} & x_3^{training\,1} & \cdots & x_r^{training\,1} \\ x_2^{training\,1} & x_3^{training\,1} & x_4^{training\,1} & \cdots & x_{r+1}^{training\,1} \\ x_3^{training\,1} & x_4^{training\,1} & x_5^{training\,1} & \cdots & x_{r+2}^{training\,1} \\ \vdots & \vdots & \vdots & \ddots & \vdots \\ x_{N-r+1}^{training\,1} & x_{N-r+2}^{training\,1} & x_{N-r+3}^{training\,1} & \cdots & x_N^{training\,1} \\ \\ x_1^{training\,2} & x_2^{training\,2} & x_3^{training\,2} & \cdots & x_r^{training\,2} \\ x_2^{training\,2} & x_3^{training\,2} & x_4^{training\,2} & \cdots & x_{r+1}^{training\,2} \\ x_3^{training\,2} & x_4^{training\,2} & x_5^{training\,2} & \cdots & x_{r+2}^{training\,2} \\ \vdots & \vdots & \vdots & \ddots & \vdots \\ x_{N-r+1}^{training\,2} & x_{N-r+2}^{training\,2} & x_{N-r+3}^{training\,2} & \cdots & x_N^{training\,2} \\ \\ x_1^{test} & x_2^{test} & x_3^{test} & \cdots & x_r^{test} \\ x_2^{test} & x_3^{test} & x_4^{test} & \cdots & x_{r+1}^{test} \\ x_3^{test} & x_4^{test} & x_5^{test} & \cdots & x_{r+2}^{test} \\ \vdots & \vdots & \vdots & \ddots & \vdots \\ x_{N-r+1}^{test} & x_{N-r+2}^{test} & x_{N-r+3}^{test} & \cdots & x_N^{test} \end{bmatrix} \quad (17)$$

Step vii: NARX model simulation and calculate RSS_{LOO}^{s} for test data set s.

Simulate the test data using equally spaced time series data recovered in step vi and parameters of the Hill equation and ARX parameters. Calculate the RSS_{LOO}^{s}, the residual sum of square for the stimulation condition of the test data set.

Step viii: Calculate RSS_{LOO} by taking the sum of RSS_{LOO}^{s} for each stimulation s.

Perform steps i to vii for all three combinations of training and test data sets. Let RSS_{LOO} be the sum of RSS_{LOO}^{s} for each stimulation *s* of test data set.

Step ix: Obtain the *Input* combination with minimum RSS_{LOO}.

Perform steps i to viii for all combinations of *Inputs*. Select the combination of *Inputs* with the minimum RSS_{LOO} for the *I-O* relationship.

Step x: Estimate the NARX model with signal recovery using all data sets.

Using the combination of *Input* determined in step ix, estimate the NARX parameter with signal recovery by the procedure from steps i to v using all stimulation conditions as training data sets.

Note that, when simulating with the ARX model, set the value of *Output* to 0 before time 0, otherwise the value of the *Output* obtained by the simulation is used to obtain the next time value. For simulation of extrapolation data set with trametinib in Figure 14, signal recovery was performed by step vi using experimental extrapolation data set with trametinib as the test data set.

2.7 Calculation of gain and time constant from the linear ARX model

Gain and time constant τ were calculated from the frequency response function obtained from the linear ARX model. For simplicity, I consider here the case of a single *Input* - single *Output* ARX model like Eq (6), which can be re-described as follows,

$$y_k - a_1 y_{k-1} - a_2 y_{k-2} - \cdots - a_{m_y} y_{k-m_y} = b_1 u_{k-1} + b_2 u_{k-2} + \cdots + b_{k-m_u}, \quad (18)$$

and its *Z*-transform are given by

$$\left(y_k - a_1 z^{-1} - a_2 z^{-2} - \cdots - a_{m_y} z^{-m_y}\right) y(z) = \left(b_1 z^{-1} + b_2 z^{-2} + \cdots + b_{m_u} z^{-m_u}\right) u(z). \quad (19)$$

Then a discrete-time transfer function, a function to convert *Input* to *Output* through the system, $G(z)$ can be described using these ARX parameters,

$$G(z) = \frac{\mathrm{y(z)}}{u(z)} = \frac{b_1 z^{-1} + b_2 z^{-2} + \cdots + b_{m_u} z^{-m_u}}{1 - a_1 z^{-1} - a_2 z^{-2} - \cdots - a_{m_y} z^{-m_y}}, \quad (20)$$

To consider the frequency response function and calculation of gain and phase, z is substituted by $i\omega$,

$$G(i\omega) = \frac{i b_1 \omega^{-1} - b_2 \omega^{-2} + \cdots + b_{m_u} (i\omega)^{-m_u}}{1 - i a_1 \omega^{-1} + a_2 \omega^{-2} - \cdots - i a_{m_y} (i\omega)^{-m_y}} \quad (21)$$

$$gain = |G(i\omega)|, phase = \angle G(i\omega) \quad (22)$$

where i is an imaginary unit and ω is frequency. The frequency response curve and phase diagram at each *Input* and *Output* of the identified linear ARX model can be also drawn by Eqs (21) and (22). Therefore, gain and phase can be calculated from ARX parameters. Note that gain calculated in this study is steady-state gain. From the frequency response function, cutoff frequency f_{cutoff}, an inverse of time constant τ, is obtained by calculating the frequency at which the gain corresponds to $\frac{1}{\sqrt{2}}$ of the steady-state gain. Because Eq (23) is established between f_{cutoff} and the time constant τ, τ can be obtained from the ARX parameters through the above procedure.

$$\tau = \frac{1}{2\pi f_{cutoff}} \quad \textbf{(23)}$$

2.8 Simulation of the integrated NARX model

The simulation can be performed by integrating the identified NARX model in this study as follows. Experimental and recovered data of pERK and pCREB, and the simulated data of c-Jun, c-Fos, Egr1, FosB, and JunB were given as *Input* data and simulation was performed using the identified NARX model in this study.

2.9 Parameter estimation environment and computational cost

Parameter estimation was performed by using 2.6 GHz CPU (Xeon E5 2670) of the super computer system of the National Institute of Genetics (NIG), Research Organization of Information and Systems (ROIS). The CPU time was 7.9 hours for the parameter estimation of the NARX model for c-Jun, c-Fos and Egr1, and CPU time was 25 hours for the parameter estimation of ODE model in the previous study which can be considered similar in the same environment (Ohashi et al., 2015) (Table 2).

2.10 Data deposit, reagent or resource list

Data deposit, reagents and resources list can be found in Table 3.

3. Results

3.1 Signal recovery using compressed sensing from unequally spaced data

In this study, I regarded unequally spaced sparse time series data as equally spaced dense time series data with missing time points, and equally spaced time series data were generated by restoring missing time points using a low-rank approach (Konishi et al., 2014). In the low-rank approach for image recovery, I assumed that the value of each pixel is represented by a linear combination of its neighbor pixels, which is mathematically represented by an autoregressive (AR) model. Then a Hankel-like matrix composed of pixel values has a low rank because each column is represented by the linear combination of the other columns (Figure 4A and Figure 5). This means that the Hankel-like matrix is a low-rank matrix whose rank is determined by the system order. Missing data can be recovered by estimating missing elements of the matrix so that the rank of this matrix [Y] is r. When system order r is unknown, based on the idea that the system can be described with as few parameters as possible, missing elements of this Hankel-like matrix are recovered so as to minimize the rank of the matrix [Y]. Based on the low rankness of the Hankel matrix, the signal recovery problem of the missing pixels can be formulated as a matrix rank minimization problem, and an image can be restored by solving this problem (Takahashi et al., 2012; Takahashi et al., 2016) (Figure 5).

I performed system identification from unequally spaced time series data of input molecules (*Inputs*) and output molecules (*Outputs*). Although an AR model is used for image recovery, I used ARX model for description of relationships between *Inputs* and *Outputs*

where the value at a time point is represented by a linear combination of two kinds of signals, *Inputs* and *Outputs*. Therefore, I modified the rank-minimization-based signal recovery method of the AR model to the ARX model and performed system identification (Figure 4B and Figure 5). Several methods for system identification employing a linear ARX model with signal recovery of missing points of input and output based on matrix rank minimization have been proposed (Liu et al., 2013). They can recover missing time series input–output data even when missing time points of input are not equal to those of output.

However, this method cannot be directly applied because I used the NARX model not but the ARX model due to the nonlinearity of signaling-dependent gene expression (Kudo et al., 2016; Saito et al., 2013). Therefore, by combining the nonlinear ARX system identification method (Saito et al., 2013) and the signal recovery method based on the matrix rank minimization problem (Konishi et al., 2014), I derived the signal recovery algorithm applicable to the nonlinear ARX system and performed system identification using recovered equally spaced time series input–output data (see "2.4 NARX Model and Data Representation" and "2.5 Extension ARX system identification from unequally spaced time series data to the NARX system" sections in Materials and methods).

3.2 System identification by integrating signal recovery and the NARX Model

In the NARX model used in the previous work, time series data of *Inputs* are nonlinearly transformed by the Hill equation, which are then used as inputs for the ARX model (Saito et al., 2013) (Figure 6A). The Hill equation, which is nonlinear transformation function $f(x)$

widely used in the field of biochemistry (Hill, 1910), can represent sensitivity with a graded or switch-like response by the values of *n* and *K* (Figure 6A). The ARX model in the NARX model can represent how the *Output* efficiently responds to the temporal change of the nonlinearly transformed *Inputs* by the time constant and gain (Figure 6A). Thus, from the estimated parameters of the Hill equation and ARX model, the sensitivity with graded or switch-like response and the time constant and gain are obtained, respectively. In this study, the parameters of this NARX model were estimated using a signal recovery scheme based on a low-rank approach (Konishi et al., 2014), as follows (Figure 6B, see details in "2.6 Procedure for system identification by integrating signal recovery and the NARX model" section in Materials and methods).

To estimate the *I-O* relationship, I selected a combination of *Inputs* for each *Output* and prepared a data set of all combinations of *Inputs* for each *Output*. Each data set was divided into test dataset for one stimulation condition and training data set for the rest of two stimulation conditions, leave-one-out (LOO) cross-validation was performed. The parameters of the NARX model (the NARX parameters) for the training data set in each *Input–Output* combination was estimated as the following method. First, the initial values of n and K are given by $n = 1$ and a random number, respectively, and nonlinear transformation of input unequally spaced time series data by the Hill equation was performed (Figure 6B, step i). A Hankel-like matrix was constructed from unequally spaced time series *Output* data and from unequally spaced time series *Inputs* nonlinearly transformed by the Hill equation. Next, signal recovery was performed with an iterative partial matrix shrinkage (IPMS) algorithm to

minimize the rank of the Hankel-like matrix composed of *Output* and *Inputs* transformed by the Hill equation (Konishi et al., 2014) (Figure 6B, step ii). The rank of the recovered Hankel-like matrix corresponds to the lag order; from the recovered Hankel-like matrix, the parameters of the ARX model $\boldsymbol{a}$ and $\boldsymbol{b}$ were uniquely obtained (Figure 6B, step iii; Figure 4B). Further estimation of n and K was performed by using recovered data, ARX parameters obtained until step iii, and other combination of n and K given random numbers (Figure 6B, step iv). By using the inverse function of the Hill equation, I recovered the missing time points data of input before transformation by the Hill equation. For the other 200 combinations of n and K given by random numbers, I performed simulation of the NARX model using the recovered data, ARX parameters obtained until step iii, and the given combination of n and K.

I calculated the Akaike information criterion (AIC) from the residual sum of squares between the experiment and simulation, number of parameters, and number of data to determine the parameters *n* and *K*. AIC is a measure of the relative quality of statistical models based on the trade-off between the goodness-of-fit of the model and the complexity of the model (Akaike, 1974). In step iv, I selected the combination of n and K with the minimum AIC and carried out signal recovery again using these n and K. I repeated steps i–iv 500 times, and selected the n and K and ARX parameters that minimize AIC for the training data set $AIC_{training}$ in total (Figure 6B, step v). Let parameters with minimum $AIC_{training}$ be parameters obtained from the training data set (Figure 6B, step v). Once these parameters were obtained, test data (still unequally spaced time series data) was added to the

recovered Hankel-like matrix and signal recovery of the test data was performed (Figure 6B, step vi). With the parameters of the NARX model estimated from the training data set, I simulated the NARX model for test data and calculated RSS_{LOO}^{s}, the residual sum of squares between experiment and simulation for test data set by stimulation condition s (NGF, PACAP, or PMA) (Figure 6B, step vii).

Because RSS_{LOO}^{s} was obtained for each combination of training and test data set s, I took the sum of RSS_{LOO}^{s} for test data set s as RSS_{LOO} (Figure 6B, step viii). I obtained the combination of *Inputs* as the identified *I-O* relationship that minimizes RSS_{LOO} for all combination of *Inputs* (Figure 6B, step ix). The *I-O* relationship indicates that a set of *Inputs* are selected as upstream molecules for each *Output*. In the final step, using this combination of input molecules, the parameters of the final NARX model were estimated by the procedure from step i to step v using all stimulation conditions as training data sets (Figure 6B, step x). Note that I used two different criterions $AIC_{training}$ and RSS_{LOO}; $AIC_{trainig}$ to determine *n*, *k*, and ARX parameters, and RSS_{LOO} to select *Inputs* in order to save computational cost.

These estimated NARX parameters were used for further study. The sensitivity with graded or switch-like response was obtained from the parameters of the Hill equation, and the gain and time constant were obtained from the parameters of the ARX model (Figure 6B, see "2.7 Calculation of gain and time constant from the linear ARX model" section in Materials and methods). An example of the transformation of *Inputs* by the Hill equation and signal recovery following the ARX model and simulated *Output* is shown in Figure 7. I applied this method to identify the signaling-decoding system by gene expression underlying cell

differentiation in PC12 cells using unequally spaced time series data with different time scales.

3.3 System identification of signaling-dependent gene expression

PC12 cells were stimulated by NGF, PACAP, and PMA and measured the amount of phosphorylated ERK1 and ERK2 (pERK) and CREB (pCREB) and protein abundance of products of the IEGs, such as c-Jun, c-Fos, Egr1, FosB, and JunB by using QIC (Ozaki et al., 2010) (Figure 8). These growth factors were chosen in this study because they activate different signaling pathways: NGF, PACAP, and PMA activates Ras-, cAMP-, and PKC-dependent signaling pathways, respectively (Farah and Sossin, 2012; Gerdin and Eiden, 2007; Ravni et al., 2006; Vaudry et al., 2002). I also measured mRNA expression of LP genes such as *Metrnl*, *Dclk1*, and *Serpinb1a* using qRT-PCR (Figure 8). I measured the signaling molecules and gene expression with different sets of the time points because of the different time scales of temporal changes in signaling molecules and gene expression (Figure 8). These measurements were carried out by the aid of liquid handling of robot (Figure 9). Using these unequally spaced time series data with the different sets of the time points, I performed the system identification employing integration of signal recovery and the NARX model (Figure 10A–C).

Using these time series data sets, I selected three sets of *Inputs–Outputs* combinations from upstream to downstream and performed system identification for each set (Figure 10A). The system identification consists of estimating the *I-O* relationship, dose-response by the Hill equation, and gain and time constant by the linear ARX model (Figure 6, see “2.7

Calculation of gain and time constant from the linear ARX model" section in Materials and methods).

I selected pERK and pCREB as *Input* candidates for each *Output*, c-Jun, c-Fos, and Egr1, based on previous studies (Akimoto et al., 2013; Saito et al., 2013; Watanabe et al., 2012) (Figure 10A). I selected pERK, pCREB, c-Jun, c-Fos, and Egr1 as *Input* candidates for each *Output*, FosB and JunB (Akimoto et al., 2013; Saito et al., 2013; Watanabe et al., 2012) (Figure 10A). I selected pERK, pCREB, c-Jun, c-Fos, Egr1, FosB, and JunB as *Input* candidates for each *Output*, *Metrnl*, *Serpinb1a*, and *Dclk1* (Watanabe et al., 2012) (Figure 10A).

For c-Jun and Egr1, pERK was selected as an *Input*, and for c-Fos, pERK and pCREB were selected as *Inputs* (Figure 10B). For FosB, c-Jun and c-Fos were selected as *Inputs*, and for JunB, pCREB was selected as *Input* (Figure 10B). For *Metrnl*, FosB, c-Fos and JunB were selected as an *Inputs*; however, contributions of c-Fos and JunB can be negligible due to their small contribution to the *Outputs* (Figure 11), indicating that a main *Input* for *Metrnl* is FosB. For *Serpinb1a* and *Dclk1*, JunB was selected as an *Input* (Figure 10B). It is noteworthy that FosB and JunB, but not signaling molecules and other IEGs, were mainly selected as *Inputs* of the LP genes and the inputs for *Metrnl* and *Dclk1* were different despite their similar temporal patterns.

I characterized the dose-response by the Hill equation and gain and time constant by the estimated linear ARX model (Figure 10C, Table 4, 5). The dose-responses from c-Jun and c-Fos to FosB showed typical switch-like responses, whereas others showed graded or weaker

switch-like responses. Note that the gain from the converted c-Jun to FosB was much smaller than that from the converted c-Fos (Table 4), indicating that FosB is mainly regulated by c-Fos but not c-Jun. The time constants for c-Jun, c-Fos, Egr1, *Metrnl*, and *Dclk1* were less than 1 h, whereas those for FosB, JunB, and *Serpinb1a* were more than 100 min (Table 4), indicating that induction of FosB and JunB temporally limit the overall induction of the LP genes from signaling molecules. The transformation of *Inputs* by the Hill equation followed by the ARX model is shown in Figure 11. The frequency response curve and phase diagram at each *Input* and *Output* of the identified linear ARX model can be also drawn, suggesting that the filter characteristics of the identified linear ARX model in this study showed low-pass filter characteristics that pass signals with a frequency lower than a certain cutoff frequency and attenuates signals with frequencies higher than the cutoff frequency. (Figure 12). In addition, when I integrated these three sets of the NARX model and simulated the response using only pERK and pCREB as *Inputs*, a similar result was obtained (Figure 13).

3.4 Prediction and validation of the identified system by pharmacological perturbation

I validated the identified system by pharmacological perturbation. One of the key issues in PC12 cell differentiation is whether ERK or CREB phosphorylation mediates expression of the downstream genes (Ravni et al., 2006; Vaudry et al., 2002; Watanabe et al., 2012). Therefore, I selectively inhibited ERK phosphorylation by a specific MEK inhibitor, trametinib (Gilmartin et al., 2011; Watanabe et al., 2013; Yamaguchi et al., 2007) in PACAP-stimulated PC12 cells. I found that PACAP-induced ERK phosphorylation, but not CREB phosphorylation, was specifically inhibited by trametinib (Figure 14A, black dots).

For c-Jun, c-Fos, Egr1, and JunB, I recovered signals of the unequally spaced time series data of *Inputs* and *Output*. For c-Jun, c-Fos, and Egr1, I simulated *Outputs* responses using these recovered data and the identified NARX model (Figure 14A black lines, see also "2.8 Simulation of the integrated NARX model" section in Materials and methods). For other downstream molecules, FosB, JunB, *Metrnl*, *Serpinb1a*, and *Dclk1*, I used the recovered data of pCREB and the simulated time series data of c-Jun, c-Fos, and Egr1 as *Inputs* for the identified NARX model (Figure 14A, black lines). The simulated time courses of *Outputs* were similar with those in experiments, except those of FosB and *Metrnl* (Figure 14A, black lines and black dots). In the simulation, FosB and *Metrnl* did not respond to PACAP in the presence of trametinib, whereas in the experiment both molecules did so, suggesting the possibility of failure of the system identification of FosB and/or *Metrnl*. Therefore, I investigated whether FosB and *Metrnl* can be reasonably reproduced when experimental and recovered data of c-Fos and c-Jun and of FosB, respectively, were used rather than the simulated ones (Figure 14B). When experimental and recovered data were used as *Inputs*, *Metrnl*, but not FosB, responded to PACAP in the presence of trametinib both in the simulation and experiment (Figure 14B), indicating that the failure of the system identification of FosB and *Metrnl* in Figure 14A arose from the failure of the system identification of FosB. Thus, all *Outputs* except FosB showed similar responses in the experiment and simulation when the experimental and recovered data were used as *Inputs*, indicating that in most cases the identified system is validated by pharmacological perturbation.

4. Discussion

4.1 Biological significance in this study

In this study, I identified the system from signaling molecules to gene expression using the unequally spaced time series data for 720 min after the stimulation. Given that expression levels of the LP genes were highly correlated with neurite length regardless of types of extracellular stimuli (Watanabe et al., 2012) and gene expression for 720 min after the initial addition of NGF or PACAP can be regarded as preparation step, latent process , for neurite outgrowth (Chung et al., 2010), the identified system is the selective growth factor–signaling decoding system for neurite length information, one of the most critical steps for cell differentiation in PC12 cells. I found that the LP genes depend only on the IEGs (c-Fos, FosB and/or JunB) but not other upstream molecules, and that the time constants of the LP genes are short except for *Serpinb1a*. This means that the timing of the final decoding step for neurite length information is not directly determined by the IEGs and LP genes, rather by the steps from growth factors to the late IEGs.

One key issue is whether ERK and/or CREB mediates cell differentiation through downstream gene expression in PC12 cells (Ravni et al., 2006; Vaudry et al., 2002; Watanabe et al., 2012). It is previously found that the LP genes are not induced by NGF in the presence of U0126, another MEK inhibitor (Watanabe et al., 2012), and that the MEK inhibitor blocks NGF-induced phosphorylation of both ERK and CREB in PC12 cells (Akimoto et al., 2013; Uda et al., 2013; Watanabe et al., 2012). By contrast, the MEK inhibitor blocked phosphorylation of ERK, but not CREB, in PACAP-stimulated PC12 cells (Akimoto et al.,

2013; Uda et al., 2013) (Figure 14), suggesting that PACAP induces phosphorylation of CREB through a cAMP-dependent pathway, rather than the ERK pathway. These results demonstrate that NGF selectively uses the ERK pathway, whereas PACAP selectively uses the cAMP pathway for induction of the LP genes. Considering that LP genes are the common decoders for neurite length in PC12 cells regardless of growth factors (Watanabe et al., 2012), the identified system in this study (except for FosB) reveals the selective NGF- and PACAP-signaling decoding mechanisms for neurite length information.

4.2 Validity of identified systems in this study

The systems leading from pERK and pCREB to the IEGs using the equally spaced dense time series data with a uniform 3-min interval during 180 min have been previously identified (Saito et al., 2013). The identified *I-O* relationships in this study are the same, except for the inputs of FosB and JunB. In this study, for FosB c-Jun was selected as an *Input* in addition to c-Fos. However, the gain from the converted c-Jun to FosB was much smaller than that from the converted c-Fos (Table 4), indicating that the effect of c-Jun is negligible. For JunB, c-Fos was not selected as an *Input* in this study, whereas c-Fos was selected in the previous study (Saito et al., 2013). The gain from the converted c-Fos to JunB at lower frequency was much smaller than that from the converted pCREB (Saito et al., 2013), indicating that the effect of c-Fos is negligible in the previous study. Thus, the identified *I-O* relationships in this study are consistent with the previous work.

The estimated NARX parameters were also generally consistent with those in the

previous study (Saito et al., 2013). The peak of c-Fos by NGF stimulation was approximately 0.9, whereas it was approximately 0.6 in the previous study (Saito et al., 2013). The difference may come from the difference in the algorithm for parameter estimation, because of the procedure of signal recovery is included in this study. Overall, the inferred the *I-O* relationship, the Hill equation, and the linear ARX model in this study are consistent with the results of the previous study, indicating that system identification using unequally spaced time series data can give the same performance as using equally spaced time series data and that the system is time invariant during 720 min. Furthermore, the identified system can reasonably reproduce the time series data using extrapolated data with trametinib, except for FosB. Taken together, these results demonstrate the validity of the predicted response of the identified systems. The reason for the failure of system identification of FosB is unclear, but it may reflect the failure of parameter estimation due to the insufficient number of experimental data points, the limitation of the NARX model structure, or the existence of unknown regulatory molecules. Further studies are necessary to address these issues.

4.3 Future works for improvement of the developed method in this study

Some of the recovered time series data is noisy such as *Metrnl* (Figure 10B), and these are possibly remedied by transforming the output of ARX model with the Hill equation instead of the inputs. However, doing so may result not only in an increasing of computational cost, but also in mathematically another two problems. First, the signal recovery cannot be applied within the present framework based on IPMS. Second, the

parameter estimation of ARX model becomes harder. The problems are essentially due to the difficulty of optimization, caused by the fact that the tuning parameters are inside nonlinear function. This transforming outputs of ARX model is a future work.

I carried out multiple-input and single-output (MISO) system identification in this study. As another improvement approach of this study method, there is multiple-input and multiple-output (MIMO) system identification. Although MIMO can be applicable, there is the combination problem between the outputs. In this study, MISO system identification was calculated in 452 combinations, but the combinations for MIMO will be increased to 1003 combinations. Also, as the number of parameters increases about twice, the cost of parameter estimation becomes more expensive. Therefore, I employed MISO system identification in this study. In addition, synergy induced by cross talk between signaling molecules is one of the most important properties in signaling network. The current NARX do not assume synergy between *Inputs* induced by such as cross talk. However, incorporation of synergy causes also combinatorial problem and increases computational cost as well as MIMO approach which considers synergy between *Outputs*. These synergistic effects should be incorporated in the future.

There are obscure points for an application of this method to biological data analysis. The relationship between a number of observed time points and accuracy of signal recovery is theoretically unknown. In addition, how to select time points is also unknown. Intuitively, dense time points may be required for transient response, while sparse time points may be sufficient for sustained response. Further study is necessary to address this issue.

4.4 Methodological significance in this study

Recent biotechnology such as fluorescence resonance energy transfer probes, optogenetics, and microfluidic devices has been developed to achieve observation and control of temporal patterns of ERK phosphorylation experimentally. These methods allow us to focus on quantitative relationships between various temporal patterns of ERK phosphorylation and phenotypes such as cell differentiation (Albeck et al., 2013; Aoki et al., 2013; Doupé and Perrimon, 2014; Ryu et al., 2015; Sumit et al., 2017; Toettcher et al., 2013; Zhang et al., 2014). Although the relationship between signal transduction such as ERK phosphorylation and phenotype has been extensively explored, it remains still unclear how the signaling molecules regulate the downstream gene expressions over a longer time scale, leading to cell fate decisions in quantitative aspects. In this study, I successfully revealed the quantitative regulatory mechanism between signaling activation at a short time scale (tens of minutes) and gene expression at a longer time scale (day) by employing a system identification method integrating a signal recovery technique and the NARX model based on compressed sensing.

A linear or spline interpolation is also used to convert unequally spaced time series data into equally spaced time series data in biological data analysis. However, such interpolation methods are not likely to be reliable because the interpolation methods ignore biochemical property of molecular network. By contrast, the signal recovery method used in this study is based on the NARX model, which reflects biochemical property. Thus, the proposal method in this study is biologically more plausible than a linear or spline interpolation.

In molecular and cellular biology, molecular networks—the *I-O* relationship in this study—are generally explored by gene disruption or pharmacological perturbation experiments, meaning that the *I-O* relationship is explored using static and qualitative data. In this study, *Inputs–Outputs* time series data for system identification allowed us to determine the *I-O* relationship, meaning that the *I-O* relationship is explored using dynamic and quantitative data. The system identification method in this study does not require detailed knowledge of pathway information, indicating that it can be used as pathway finding directly from time series data. Moreover, additional information such as sensitivity with graded or switch-like response, time constant, and gain can be obtained. One of the advantages of using time series data rather than static qualitative data is simultaneously obtaining the *I-O* relationship, sensitivity, and time constant, which characterize the system behavior. This is based on the idea that input–output time series data implicitly include information of the *I-O* relationship. However, it must be noted that the *I-O* relationship obtained by employing this method may be an apparent relationship inferred from time series data and does not necessarily correspond to the direct *I-O* relationship. Therefore, the obtained *I-O* relationship should be validated by gene disruption or pharmacological perturbation experiments, as conducted in Figure 14.

To summarize the above points, as caveats when employing NARX model, estimated *I-O* relationships is phenomenological relationship, rather than direct interaction (Table 2). Furthermore, the possibility that unknown molecules are upstream inputs cannot be ruled out. On the other hand, even if the pathway is unknown and the prior knowledge is not available, the model candidates can be prepared systematically in the NARX model, which is suitable for

estimating *I-O* relationships. In particular, in the case of estimating *I-O* relationships including nonlinear biochemical reactions without detailed prior knowledge like in this study, the estimation of *I-O* relationships by ODE model is difficult and NARX model is useful. I also compared the parameter estimation cost between the NARX model for c-Jun, c-Fos and Egr1 and ODE model in previous study because the model size can be considered similar (Ohashi et al., 2015), indicating that the parameter estimation cost of NARX model in this study is relatively small. In addition to that, the system identification method in this study overcomes the limitation of the NARX model which requires equally spaced dense time series data, and it is possible to apply to unequally spaced time-series data. Although it is difficult to obtain the direct mechanistic interactions by the NARX model, the result of the *I-O* relationships and time constants provided biological insight of decoding mechanism of the upstream molecules by the LP genes expression.

4.5 Summary and conclusions

In conclusions, I have developed a system identification method using unequally spaced sparse time series data combined by signal recovery. Due to technical and budget limitations in biological experiments, it is generally difficult to obtain sufficient numbers of equally spaced dense time series data of molecules with different time scales. Thus far, system identification based on time series data has been limited to phenomena with similar time scales. However, the system identification method in this study can solve this time-scale problem and can be broadly applied to different time scale biological phenomena, such as the

cell cycle, development, regeneration, and metabolism involving ion flux, metabolites, and gene expression. Thus, I provide a versatile method for system identification of various biological phenomena using data with different time scales.

5. Figures

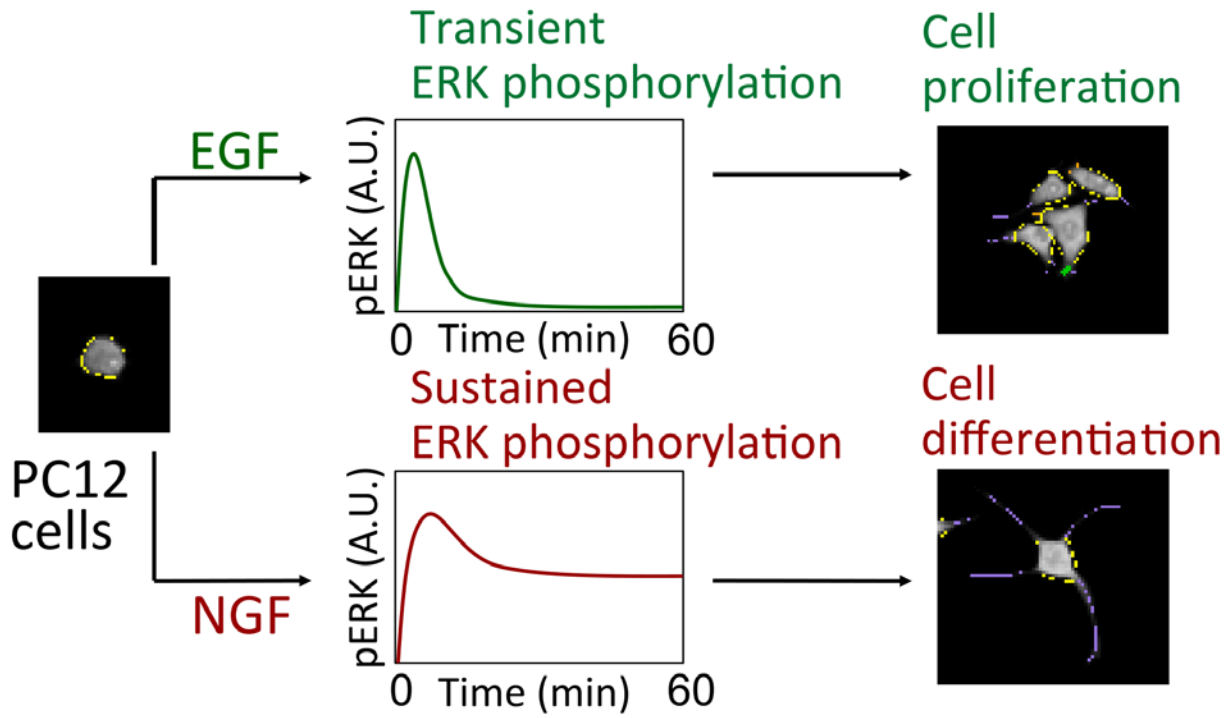

Figure 1. Schematic overview of temporal coding in PC12 cell fate decisions.

In rat adrenal pheochromocytoma PC12 cells, it has been reported that epidermal growth factor (EGF) induces cell proliferation thorough transient phosphorylation of ERK, whereas nerve growth factor (NGF) induces cell differentiation through sustained phosphorylation of ERK. This phenomenon can be regarded that information of extracellular stimuli is once encoded into temporal patterns of ERK phosphorylation and decoded into each cell fate decision.

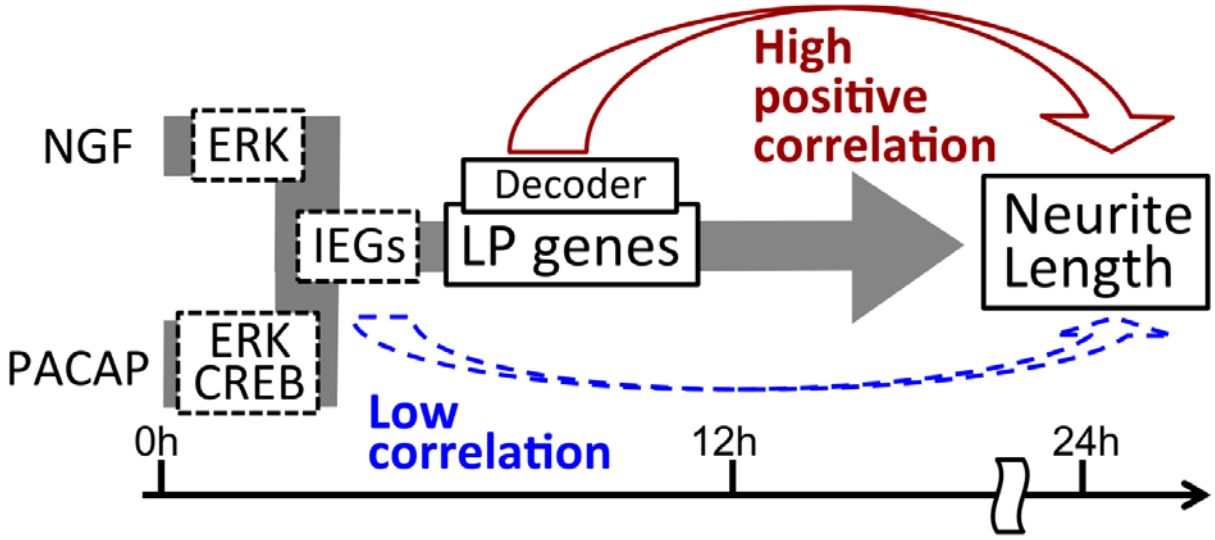

Figure 2. Schematic overview of previously identified LP genes as decoder of neurite length information.

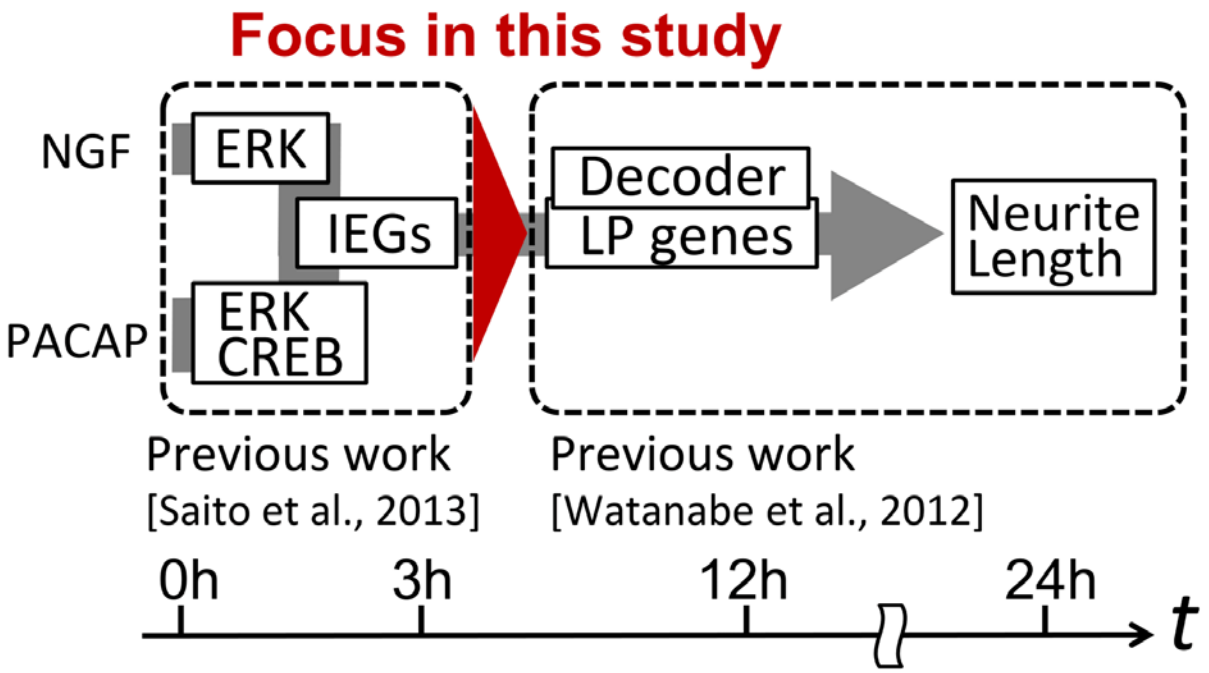

Figure 3. Schematic overview of focus in this study.

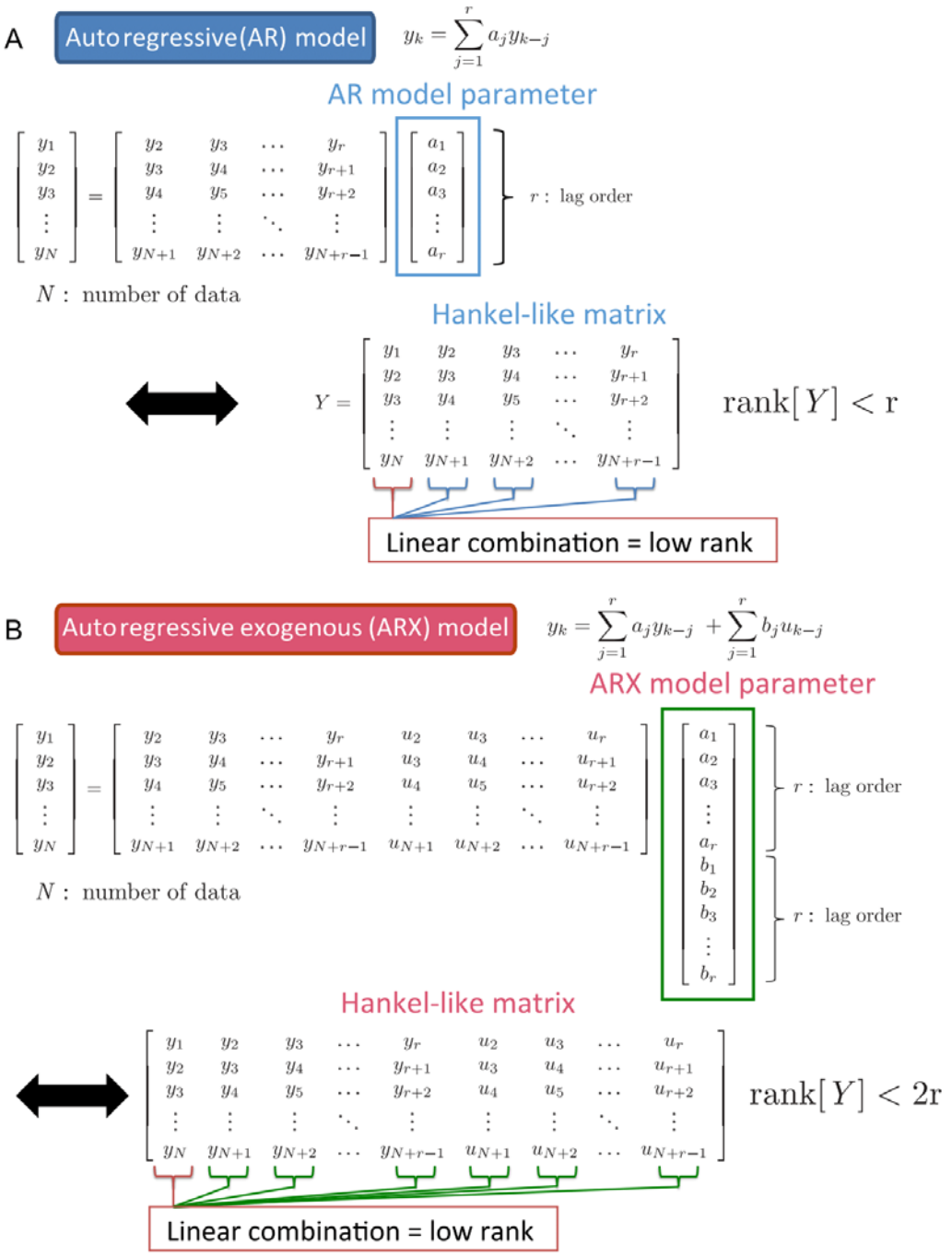

Figure 4. Estimation of AR or ARX parameters by rank minimization of Hankel-like matrix.

(**A**) Estimation of AR parameters by rank minimization of Hankel-like matrix. When the signal y follows an AR model, y_1 is represented by the linear sum from y_2 to y_r where r is lag order. This relationship can be expressed using AR parameters as the first row of the above matrix equation. Similarly, y_2 is represented by the linear sum from y_3 to y_{r+1} as

expressed in the second row. Therefore, for number of data N, the matrix equation is established as shown in the above formula. Given that this matrix equation holds, in the Hankel-like matrix below, the first column is represented by the linear sum of the second and subsequent columns, indicating that the matrix is a low-rank matrix. Note that Hankel-like matrix is a one in which the same components are entered from the lower left to the upper right here. Therefore, assuming that y follows an AR model, in case that there is missing data in y, it can be recovered by minimizing the rank of this Hankel-like matrix. Once the Hankel-like matrix is obtained, AR parameters can be estimated by solving the above matrix equation. (**B**) Estimation of ARX parameters by rank minimization of a Hankel-like matrix. In the case of ARX model with input u added, the similar Hankel-like matrix composed of y and a Hankel-like matrix composed of u, and the matrix equation of the above equation are established. Assuming that y and u follow the ARX model, missing data in y and u can be recovered by minimizing the rank of this Hankel-like matrix, and ARX parameters can be estimated by solving the above matrix equation. Note that this method can be applicable for multiple inputs by increasing the number of Hankel-like matrices composed of u.

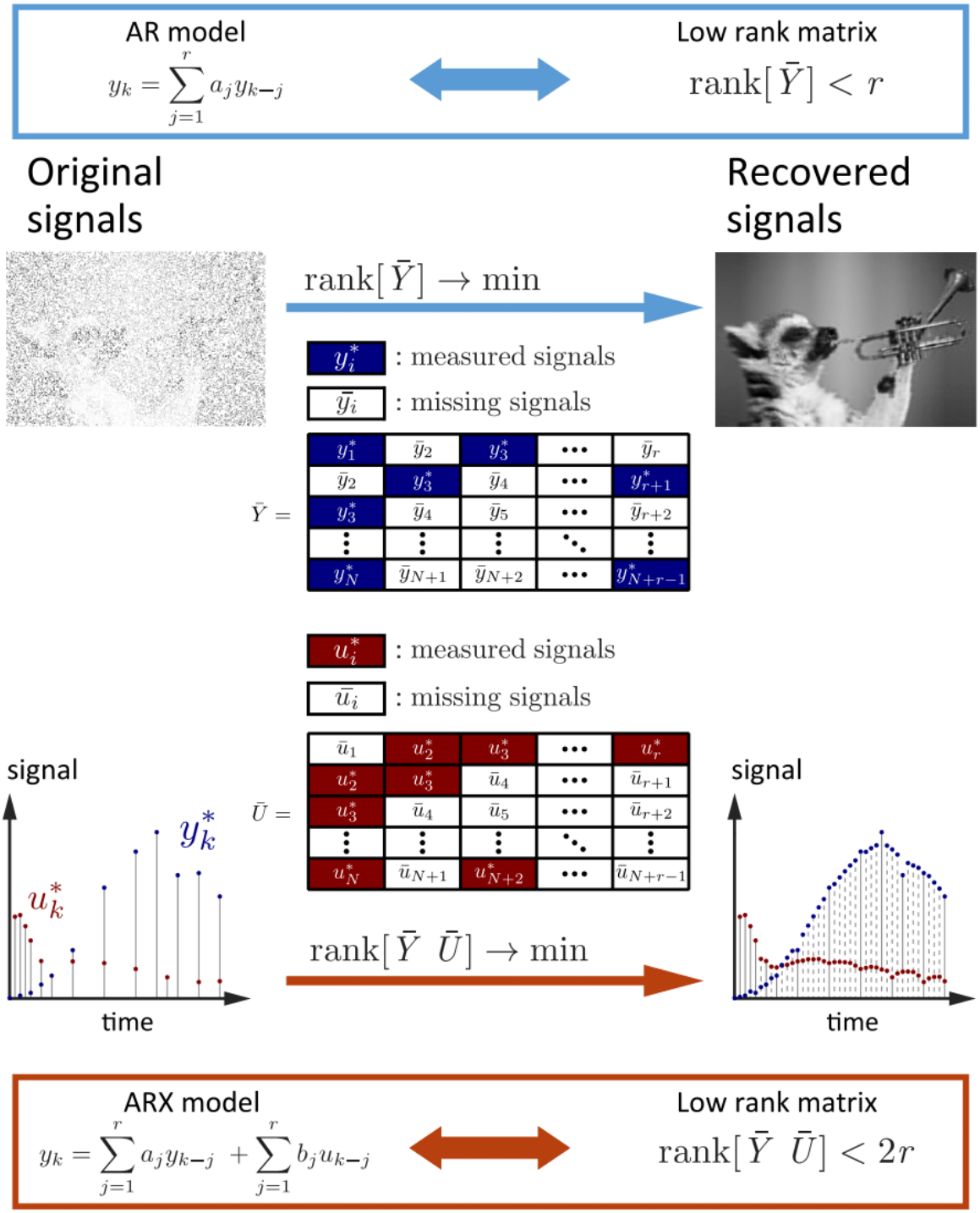

Figure 5. Signal recovery based on compressed sensing technology from unequally spaced data.

(**Top**) An example of recovered equally spaced image data from unequally spaced image data by the signal recovery technique using rank minimization of the Hankel-like matrix ***Y*** composed of signals in pixels. I assume that the value of each pixel is represented by a linear

combination of those of its neighboring pixels, which is mathematically represented by an autoregressive (AR) model. The original picture is published under the Creative Commons Zero license in https://www.pexels.com/photo/animal-black-and-white-cute-funny-164703/. (**Bottom**) An example of recovered equally spaced time series data from unequally spaced time series data by the signal recovery technique using rank minimization of the Hankel-like matrices $\boldsymbol{Y}$ and $\boldsymbol{U}$, composed of time series data of input molecules (*Inputs*) and output molecules (*Outputs*), respectively. I assume that the value at a certain time is represented not only by the linear combination of values of the output molecule at past points but also by the linear combination of the values of the input molecule at past points, which is mathematically represented by an autoregressive exogenous (ARX) model. The recovered time series input–output data have the equally spaced time series data with the same time points even if the missing time points of input and output are different.

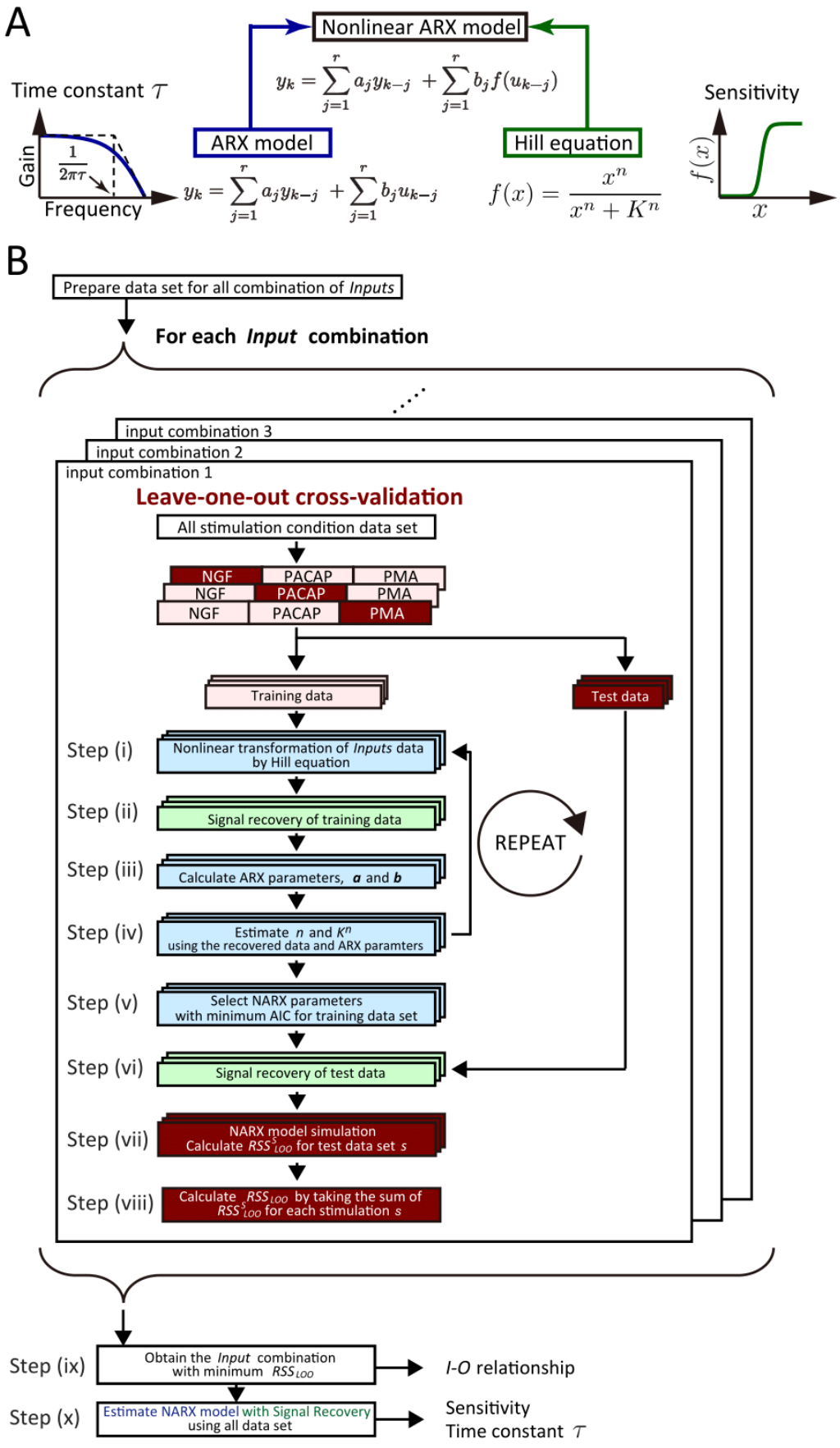

Figure 6. System identification by integrating signal recovery and the NARX model.

(**A**) The nonlinear ARX (NARX) model consists of static nonlinear conversion of input signal by the Hill equation, followed by time delay by ARX model. The former gives the sensitivity with a graded or switch-like response and the latter gives the time constant. (**B**) Algorithm flowchart for system identification by integrating signal recovery and the NARX model. See details in “2.6 Procedure for system identification by integrating signal recovery and the NARX model” section in Materials and methods.

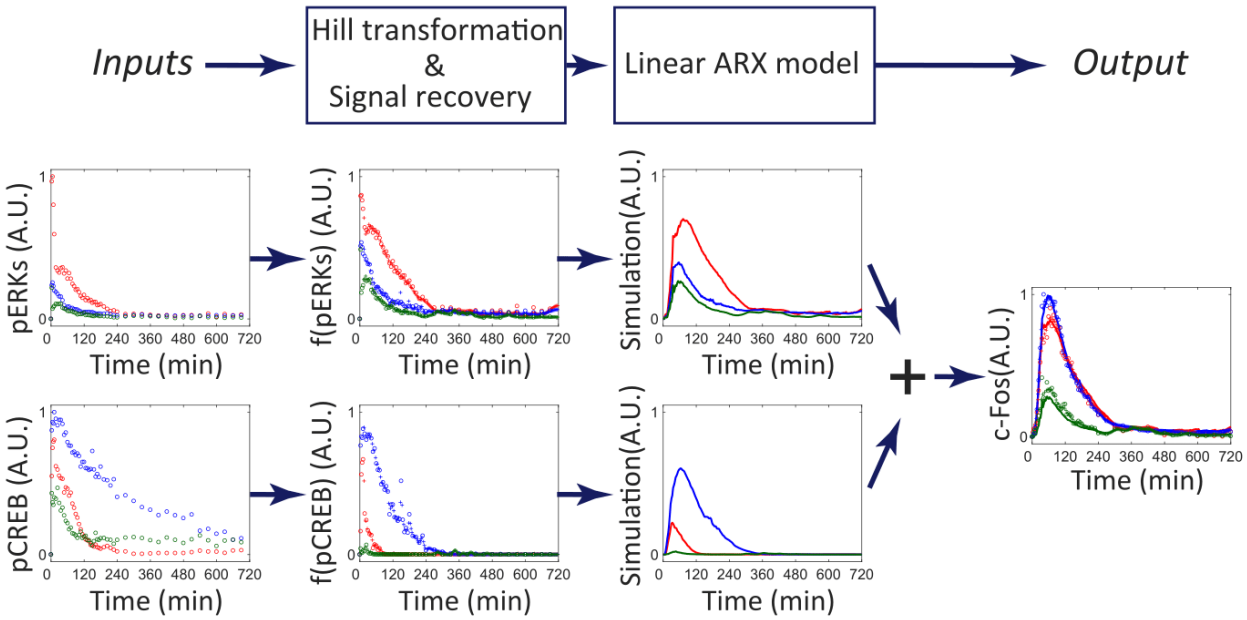

Figure 7. Transformation of *Inputs* by the Hill equation and signal recovery followed by the ARX model.

Signal transformation in the nonlinear ARX model of c-Fos is shown. The signals of pERK and pCREB were transformed by the Hill equations and recovered. Then the transformed signals were temporally transformed by the linear ARX model. The sum of the transformed signals by the linear ARX model was c-Fos, the final output of the nonlinear ARX model of c-Fos.

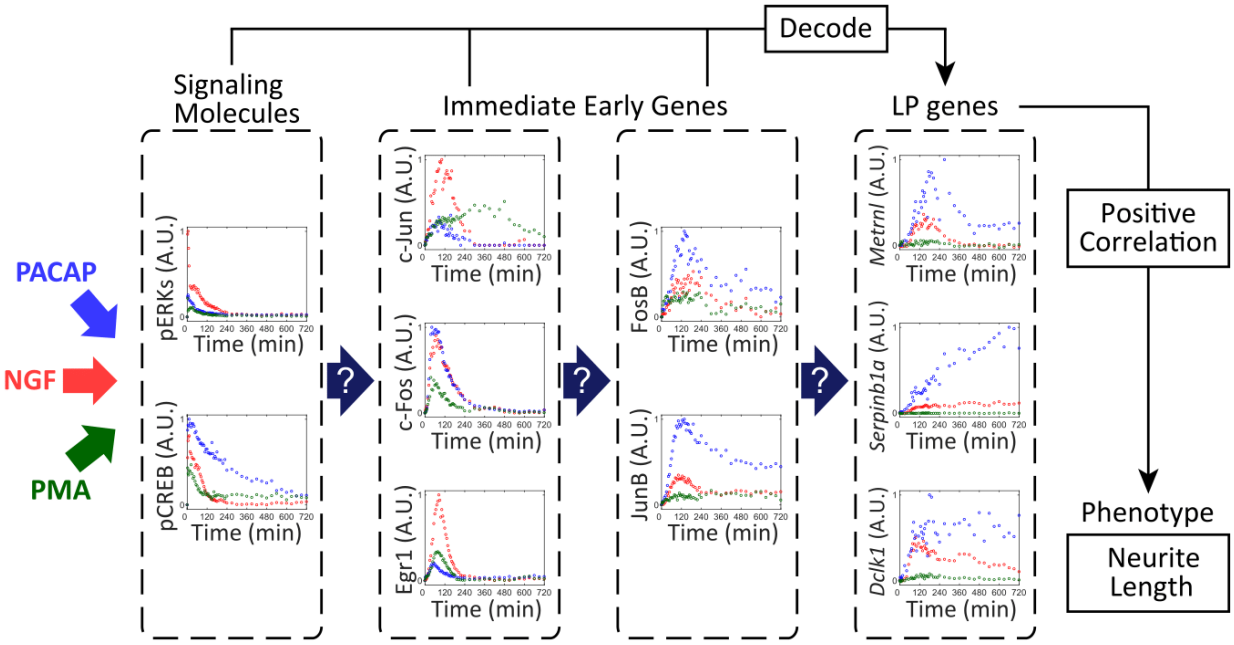

Figure 8. Experimental data of growth factor–dependent changes of signaling molecules and gene expression in PC12 cells.

PC12 cells were stimulated with NGF (50 ng/ml, red), PACAP (100 nM, blue), or PMA (100 nM, green). Phosphorylation of signaling molecules, such as ERK and CREB, the product of IEGs such as c-Jun, c-Egr1, c-Jun, FosB, and JunB, and mRNA expression of LP genes such as *Metrnl*, *Dclk1*, and *Serpinb1a* were measured with different time points. These data were used for system identification by the NARX model in Figure 10A–C.

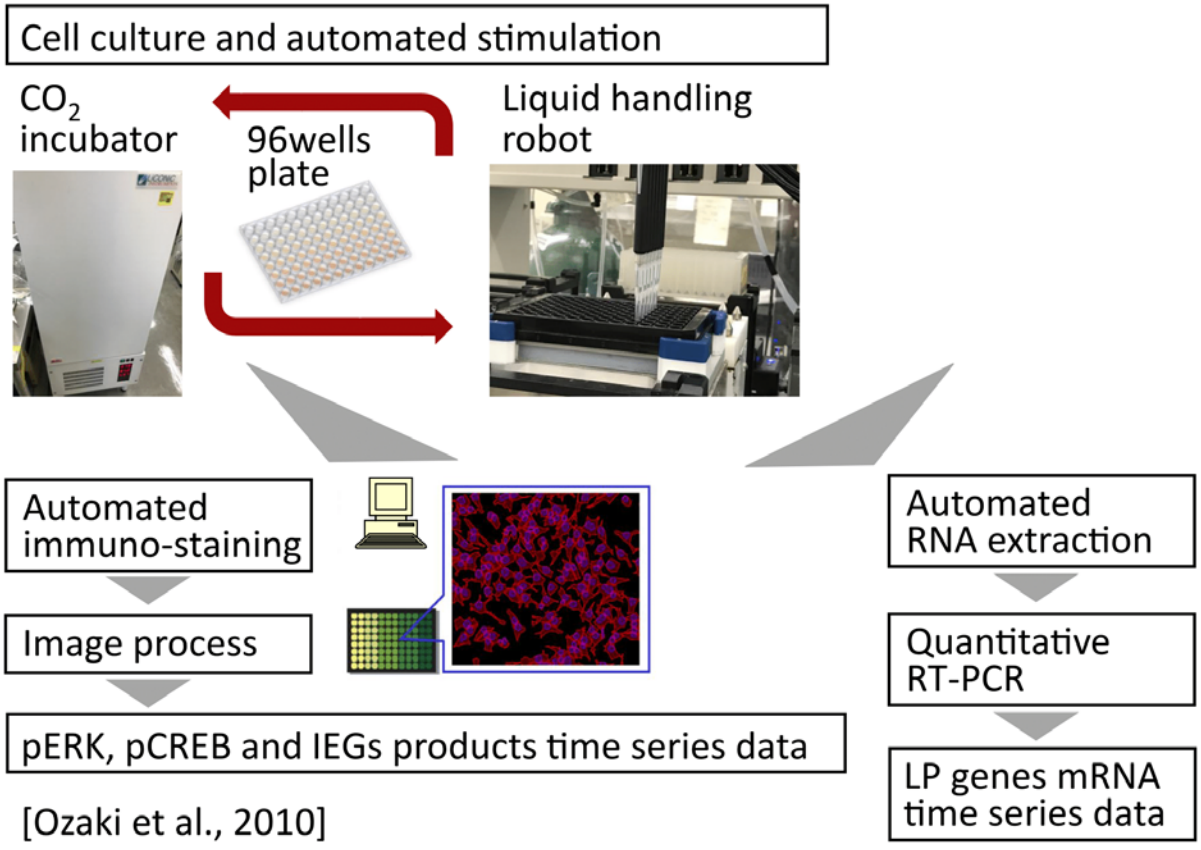

Figure 9. Measurement flow of time series data for system identification.

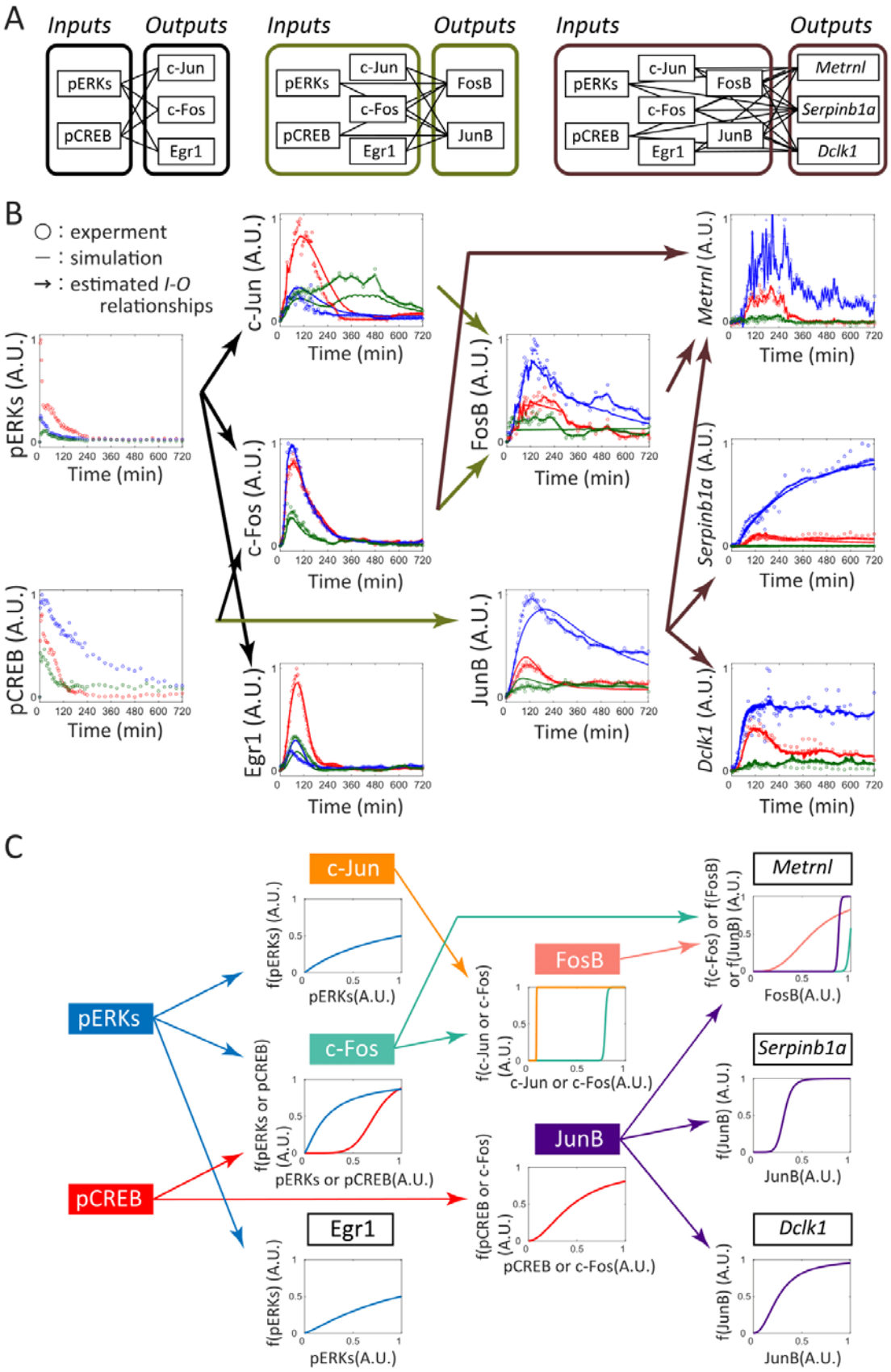

Figure 10. System identification of *I-O* relationships between the signaling, IEGs, and LP genes.

(**A**) The sets of combinations of *Inputs* and *Outputs* for system identification. (**B**) The identified *I-O* relationships. Arrows indicate the estimated *I-O* relationships for each set of inputs and outputs. The colors of the arrows indicate the same sets of combinations of inputs and outputs as in (A). Dots, experimental data; pluses, the recovered signal data; solid lines, simulation data of the NARX model; red, NGF stimulation; blue, PACAP stimulation; green, PMA stimulation. (**C**) The dose-response curves obtained by the Hill equation. For each panel, conversion of *Inputs* by the identified Hill equation is shown. The colors of the arrows and plotted lines indicate the same *Inputs*, respectively.

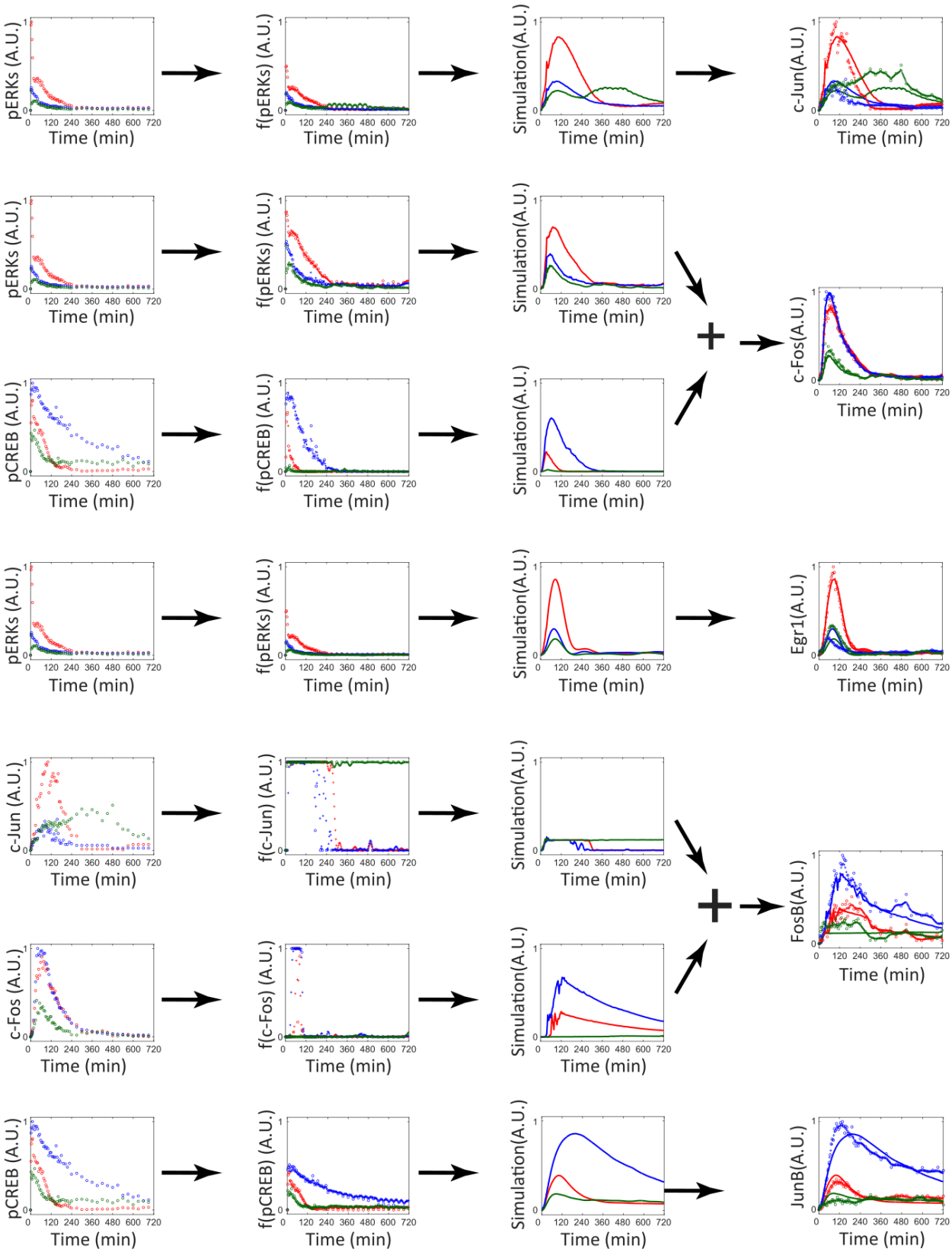
pERKs (A.U.)
f(pERKs) (A.U.)
Simulation(A.U.)
c-Jun(A.U.)
pERKs (A.U.)
f(pERKs) (A.U.)
Simulation(A.U.)
pCREB (A.U.)
f(pCREB) (A.U.)
Simulation(A.U.)
c-Fos(A.U.)
pERKs (A.U.)
f(pERKs) (A.U.)
Simulation(A.U.)
Egr1(A.U.)
c-Jun (A.U.)
f(c-Jun) (A.U.)
Simulation(A.U.)
c-Fos (A.U.)
f(c-Fos) (A.U.)
Simulation(A.U.)
FosB(A.U.)
pCREB (A.U.)
f(pCREB) (A.U.)
Simulation(A.U.)
JunB(A.U.)
Time (min)
0 120 240 360 480 600 720

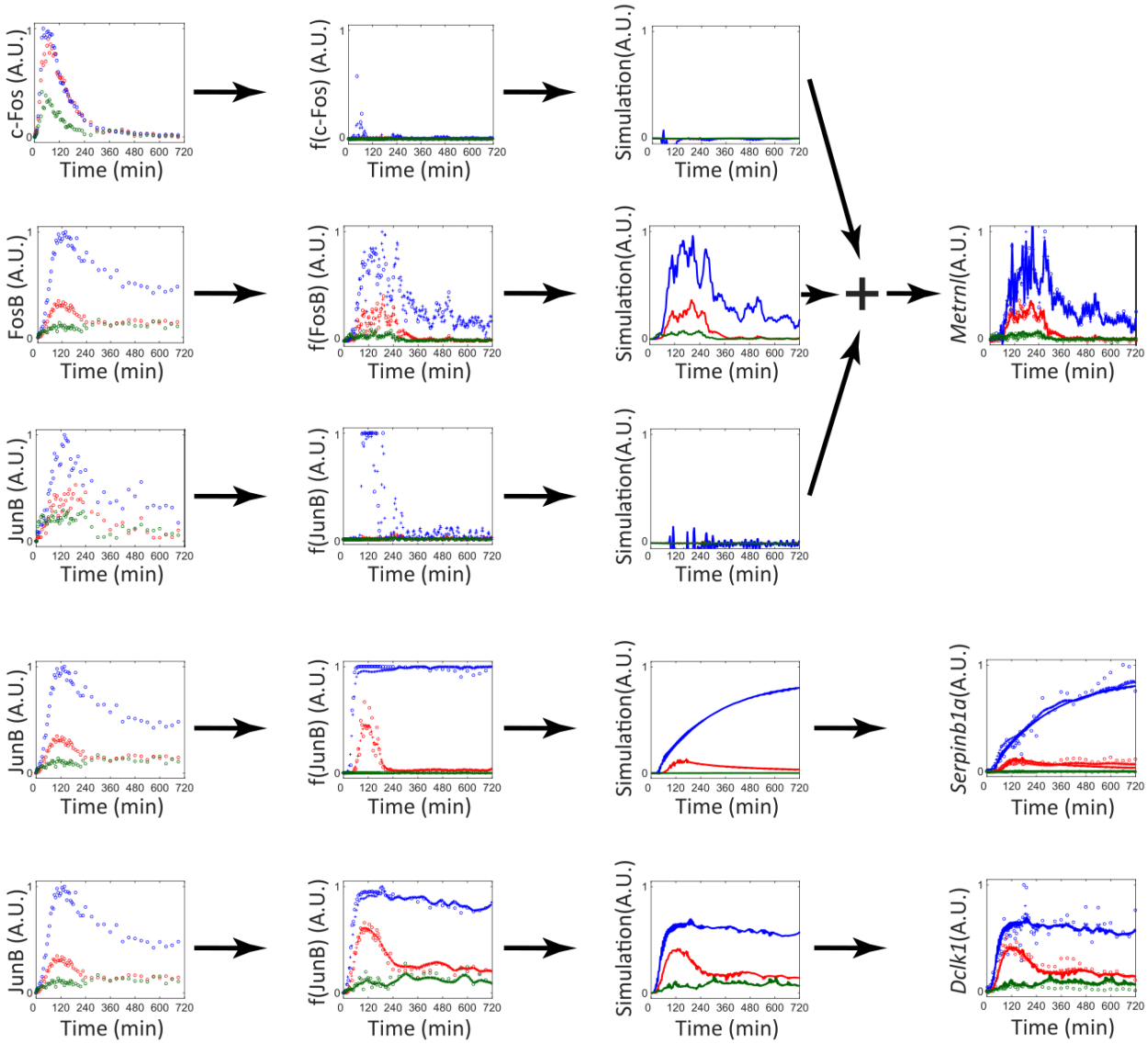

Figure 11. Transformation of *Inputs* by the Hill equation followed by the ARX model for each *Output*.

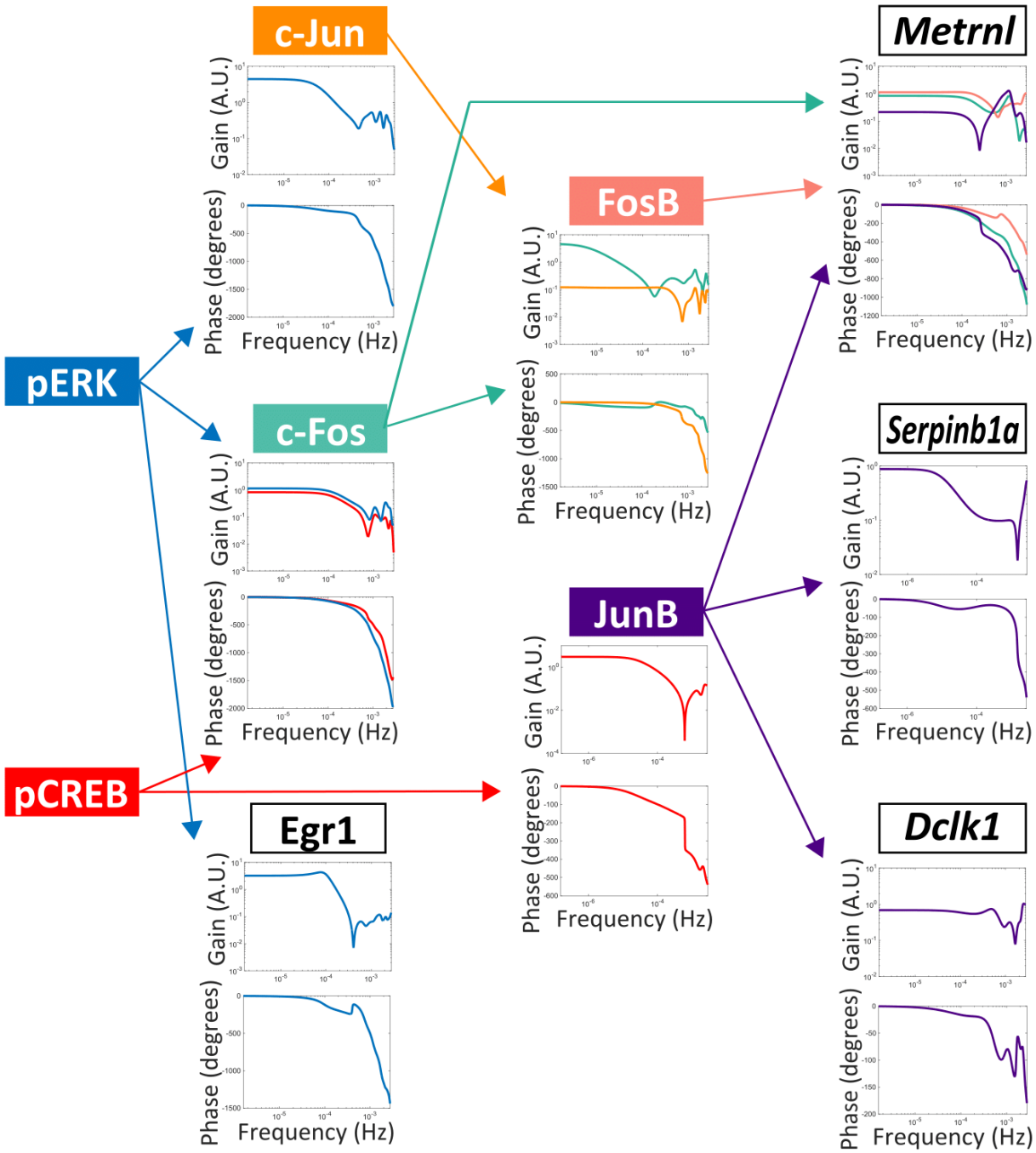

Figure 12. Frequency response curve and phase diagram at each *Input* and *Output* of the identified linear ARX model.

The frequency response curves (upper panel for each) and phase plots (lower panel for each) of the identified linear ARX models in Figure10A–C are shown for each output. Arrows indicate the identified *I-O* relationships in Figure 10A–C. The colors of the arrows and

plotted lines indicate the same input molecules, respectively. Gains and time constants of the linear ARX model are shown in Table 4. Filter characteristics of frequency response curves of these outputs showed low-pass filter characteristics.

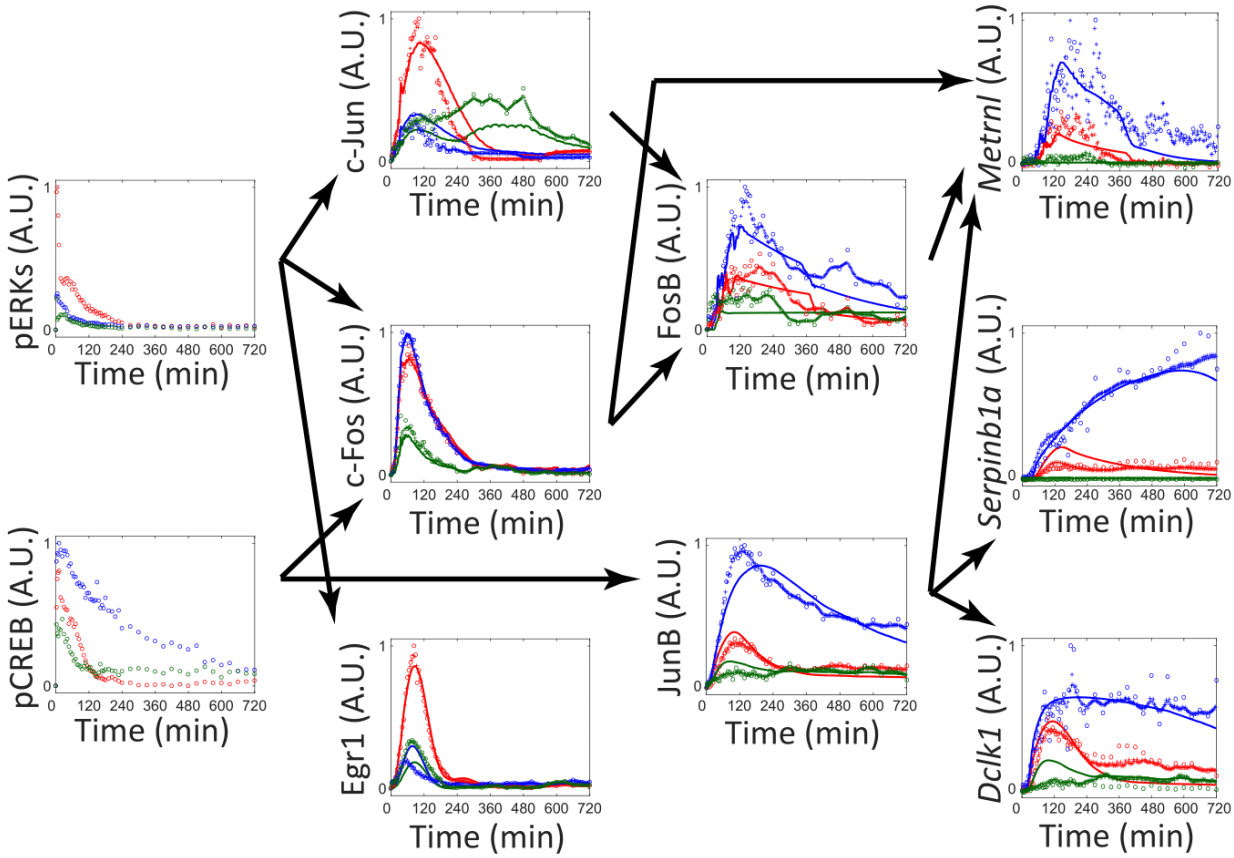

Figure 13. Simulated responses in the integrated NARX model.

Solid lines, the simulation results by the integrated NARX model identified in Figure 10 using only pERK and pCREB as *Inputs* (see "2.8 Simulation of the integrated NARX model" section in Materials and methods); dots, experimental data; pluses, the recovered signal data; red, NGF stimulation; blue, PACAP stimulation; green, PMA stimulation.

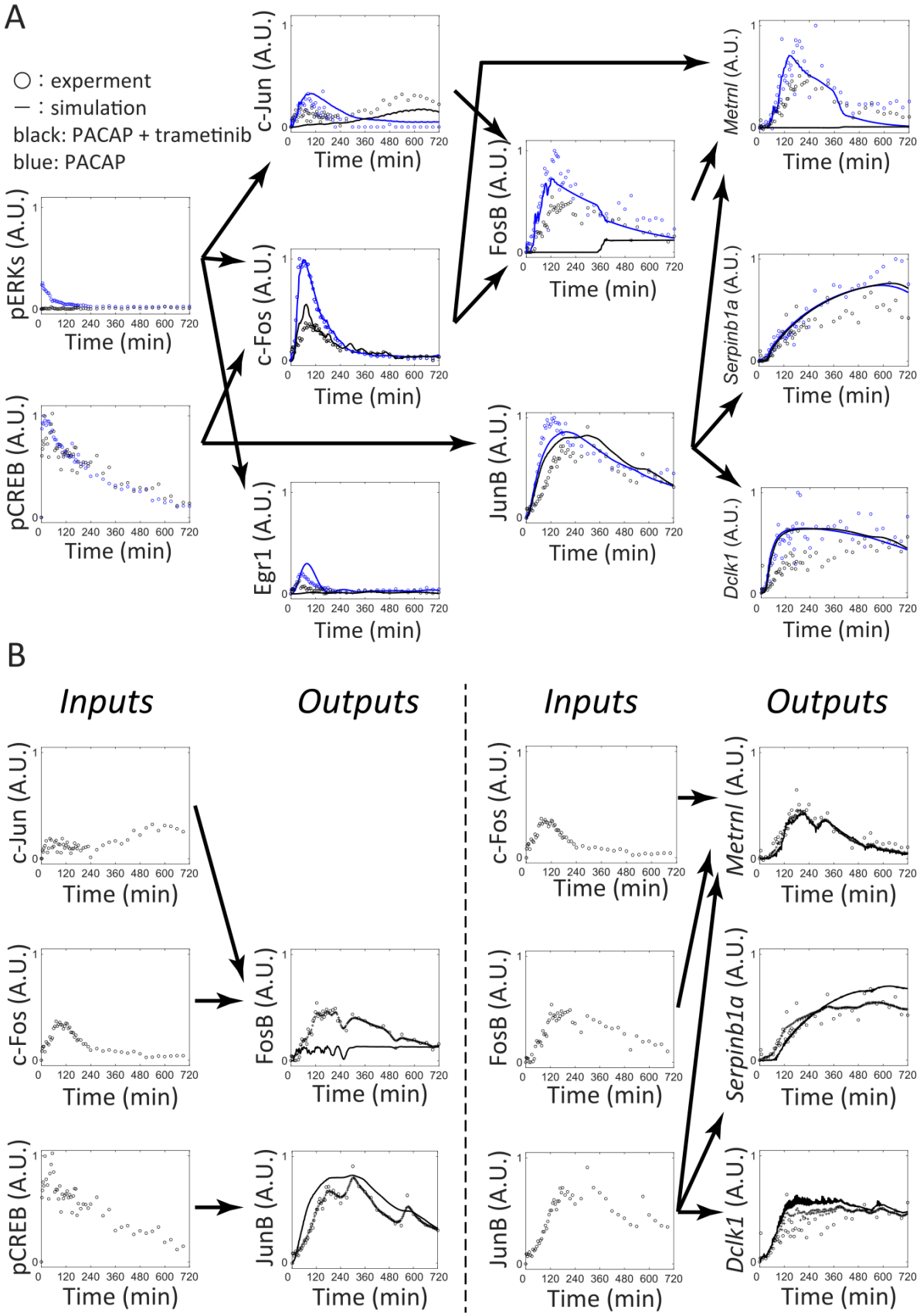

Figure 14. Prediction and validation of the identified system by pharmacological perturbation.

(**A**) The predictive simulation result and experimental result by PACAP stimulation in the presence (black) or absence (blue) of trametinib. Lines, simulation; dots, experimental and recovered data. Experimental and recovered data of pERK and pCREB, and the simulated data of c-Jun, c-Fos, Egr1, FosB, and JunB are given as *Inputs*, and simulation was performed using the NARX model in Figure 10 (see "2.8 Simulation of the integrated NARX model" section in Material and methods). In the experiment, PC12 cells were treated in the absence (blue dots) or in the presence (black dots) of trametinib (10 μM) added at 30 min before stimulation with PACAP (100 nM). Note that the PACAP stimulation data are used, as in Figure 8. (**B**) Simulation using experimental and recovered data as *Inputs*. For each set of the *Inputs* (left panel for each) and *Outputs* (right panel for each), the unequally spaced time series data were recovered (pluses) (right panel for each), and the responses of *Outputs* were simulated by the NARX model identified in Figure 10A–C (solid lines) (right panel for each).

6. Tables

Table 1. The primer sequences used for qRT-PCR.

Gene	Forward	Reverse
Actb	CCCGCGAGTACAACCTTCT	CGTCATCCATGGCGAACT
Metrnl	CGGCCCAACACCTTCTCA	CCCCAGAGGAGTCCCTGAA
Serpinb1a	TGGGTGTGGTGGACAGCAT	CTCCCACATCCCCTTGAAGTAG
Dclk1	GGCTATTGTCAGGTCA	AGTGGAGAGCTGACTG

Table 2. The comparison of NARX and ODE modeling frameworks.

	NARX modeling in this study	ODE modeling
Model candidates	Systematic representation	NOT obvious
Sampling design	Unequally and equally spaced time series data	Unequally and equally spaced time series data
Parameter estimation cost	Small computational cost 7.9 hours of CPU time for c-Jun, c-Fos and Egr1 estimation in this study	Large computational cost 25 hours of CPU time in the previous study (Ohashi et al., 2015)
Biological interpretation	Phenomenological relationship	Mechanistic interaction

Table 3. Data deposit, reagents and resources list.

DATA DEPOSIT, REAGENT or RESOURCE	SOURCE	IDENTIFIER
Data deposit		
Data files used in this study	Kuroda laboratory database	http://kurodalab.bs.s.utokyo.ac.jp/info/Tsuchiya/
Antibodies		
Mouse anti-phospho-ERK1/2 (Thr 202/Tyr 204)	Cell Signaling Technology	Cat: 9106; RRID: AB_331768
Rabbit anti-phospho-CREB (Ser 133)	Cell Signaling Technology	Cat: 9198; RRID: AB_2561044
Rabbit anti-c-Jun	Cell Signaling Technology	Cat: 9165; RRID: AB_2130165
Rabbit anti-c-Fos	Cell Signaling Technology	Cat: 2250; RRID: AB_2247211
Rabbit anti-Egr1	Cell Signaling Technology	Cat: 4154; RRID: AB_2097035
Rabbit anti-FosB	Cell Signaling Technology	Cat: 2251; RRID: AB_2106903
Rabbit anti-JunB	Cell Signaling Technology	Cat: 3753; RRID: AB_2130002
Alexa 488 goat anti-mouse IgG (H+L)	Invitrogen	Cat: A11029; RRID: AB_138404
Alexa 546 goat anti-rabbit IgG (H+L)	Invitrogen	Cat: A11035; RRID:AB_143051
Chemicals, Peptides, and Recombinant Proteins		
DMEM	Sigma	Cat: D6046
Horse serum	Gibco	Cat: 16050-122
Fetal bovine serum	Sigma	Cat: 172012
NGF	R&D Systems	Cat: 1156-NG
PACAP	Sigma	Cat: A1439
PMA	Sigma	Cat: P1585
Trametinib	Selleckchem	Cat: S2673
poly-L-lysine	Sigma	Cat: P4707
Power SYBR Green PCR Master Mix	Applied Biosystems	Cat: 4367659
Can Get Signal immunostain solution A	Toyobo	Cat: NKB-501
Hoechst 33342	Invitrogen	Cat: H-3570
Critical Commercial Assays		
High Capacity RNA-to-cDNA Kit	Applied Biosystems	Cat: 4387406

Agencourt RNAdvance Tissue Kit	Beckman Coulter	Cat: 32646
Experimental Models: Cell Lines		
PC12 rat adrenal pheochromocytoma cells	Masato Nakafuku (Ohio) Sasagawa et al., 2005	N/A
Oligonucleotides		
Primers for qRT-PCR, see Table 1	This thesis	N/A
Software and algorithms		
7300 System SDS software version 1.3.1.21	Applied Biosystems	N/A
Iterative partial matrix shrinkage algorithm	Konishi et al., 2014	http://dx.doi.org/10.1016/j.sigpro.2014.01.014
MATLAB	MathWorks	https://www.mathworks.com/
Other		
CellInsite NTX	Thermo Fisher Scientific	N/A
7300 Real Time PCR System	Applied Biosystem	N/A
Biomek NX Span-8 liquid handling system	Beckman Coulter	N/A
Thermoshake heater-shaker	Variomag	Model number: 7100146-B
Robotic incubator STX-40	Liconic	N/A

Table 4. The identified I-O relationships, parameters of the Hill equation, and gain and time constant calculated from the linear ARX model in Figure 10.

***I-O* relationship**		**Hill equation**		**Linear ARX model**	
Input	Output	*K* (EC50)	*n* (Hill	Gain	Time constant (min)
pERK	c-Jun	0.9999	1	4.4315	56.4
pERK	c-Fos	0.2274	1.276	1.137	20.8
pCREB	c-Fos	0.7189	6.118	0.8218	22
pERK	Egr1	0.998	1.225	3.2058	21.3
c-Fos	FosB	0.792	81.79	4.682	413
c-Jun	FosB	0.0813	78.58	0.1215	6.5
pCREB	JunB	0.9733	1.58	2.9857	108.9
c-Fos	*Metrnl*	0.9948	60.7	0.8347	16.8
FosB	*Metrnl*	0.5998	3.01	1.1256	10.7
JunB	*Metrnl*	0.8735	89.61	0.2128	21.7
JunB	*Serpinb1a*	0.3161	7.594	0.8797	275.4
JunB	*Dclk1*	0.2584	2.234	0.6889	4

Table 5. The parameters of the linear ARX model in the identified NARX model.

Output: c-Jun		Parameters of linear ARX model							
Lag numbers		0	1	2	3	4	5	6	7
a	c-Jun	1	-0.05636	-0.07904	0.07393	0.07073	-0.092	0.11653	-
b	f(pERK)	0	0.05203	0.02569	-0.26892	0.01635	0.19511	-0.06765	0.12280
Lag numbers		8	9	10	11	12	13	14	15
a	c-Jun	0.19058	-0.19643	0.20707	-0.19744	0.30607	-0.25843	1.01235	
b	f(pERK)	-0.04977	-0.00182	0.03571	-0.01791	-0.01323	0.08672	0.03862	

Output: c-Fos		Parameters of linear ARX model							
Lag numbers		0	1	2	3	4	5	6	7
a	c-Fos	1	-0.07786	0.05640	-0.03457	0.20982	-0.25842	0.05571	-
b	f(pERK)	0	-0.02653	0.03919	-0.0189	-0.04503	0.01806	0.03843	0.02686
	f(pCREB)	0	-0.14776	0.11187	0.03756	-0.0264	0.06621	-0.00505	0.02779
Lag numbers		8	9	10	11	12	13	14	15
a	c-Fos	0.25225	-0.32325	0.25983	0.00353	0.76672			
b	f(pERK)	-0.01283	0.02310	0.01944	0.03389	0.00123			
	f(pCREB)	0.05852	-0.00038	-0.00855	-0.00307	0.02336			

Output: Egr1		Parameters of linear ARX model							
Lag numbers		0	1	2	3	4	5	6	7
a	Egr1	1	0.02803	-0.18123	0.17547	-0.18934	0.10918	-0.08113	0.01620
b	f(pERK)	0	0.07552	-0.01501	0.00001	-0.00963	0.08151	-0.04199	0.04984
Lag numbers		8	9	10	11	12	13	14	15
a	Egr1	0.09142	-0.16053	0.26214	-0.03481	0.89833			
b	f(pERK)	0.00044	0.02653	0.02436	-0.01258	0.03326			

Output: FosB		Parameters of linear ARX model							
Lag numbers		0	1	2	3	4	5	6	7
a	FosB	1	0.19003	-0.24571	0.07129	-0.01971	0.11284	-0.13632	0.13473
b	f(c-Jun)	0	0.05394	-0.03018	0.09950	-0.12046	0.03169	0.00311	0.07020
	f(c-Fos)	0	0.00565	-0.03262	0.03497	-0.04145	-0.00351	-0.01137	0.02890
Lag numbers		8	9	10	11	12	13	14	15
a	FosB	-0.04834	0.23658	0.12791	0.56110				
b	f(c-Jun)	-0.15959	-0.07944	0.14646	0.05768				
	f(c-Fos)	-0.00751	0.00366	-0.01483	0.03999				

Output: JunB		Parameters of linear ARX model							
Lag numbers		0	1	2	3	4	5	6	7
a	JunB	1	-0.16094	0.03511	-0.05582	0.22319	0.34363	0.58953	
b	f(pCREB)	0	-0.00514	0.04735	-0.01353	0.03670	-0.06704	0.07713	
Output: *Metrnl*		Parameters of linear ARX model							
Lag numbers		0	1	2	3	4	5	6	7
a	*Metrnl*	1	-0.04026	-0.0151	0.03295	0.03830	-0.12754	0.03487	0.27308
b	f(c-Fos)	0	-0.04262	-0.0351	0.01562	0.05813	-0.13385	-0.08975	0.04191
	f(FosB)	0	-0.12975	0.18138	-0.17231	0.14247	-0.24007	0.56277	-
	f(JunB)	0	0.02934	0.01836	-0.14392	-0.0257	0.01617	0.13484	0.17338

Lag numbers		8	9	10	11	12	13	14	15
a	*Metrnl*	0.01394	-0.48672	1.11197					
b	f(c-Fos)	0.10183	0.00285	-0.05637					
	f(FosB)	0.48180	-0.04295	0.06256					
	f(JunB)	-0.23443	-0.07181	0.06872					

Output: *Serpinb1a*		Parameters of linear ARX model							
Lag numbers		0	1	2	3	4	5	6	7
a	*Serpinb1a*	1	0.33324	0.14961	0.30528	0.18354			
b	f(JunB)	0	-0.10909	0.09347	-0.06756	0.10808			

Output: *Dclk1*		Parameters of linear ARX model							
Lag numbers		0	1	2	3	4	5	6	7
a	*Dclk1*	1	0.08028	-0.00022	0.06317	-0.10167	0.07480	-0.15236	0.05486
b	f(JunB)	0	0.07328	-0.12492	0.06225	-0.12569	0.14993	-0.26375	0.20657
Lag numbers		8	9	10	11	12	13	14	15
a	*Dclk1*	0.31004	0.37326						
b	f(JunB)	-0.17042	0.39791						

7. References

Akaike, H. (1974). A new look at the statistical model identification. IEEE Trans Automat Control *19*, 716–723.

Akimoto, Y., Yugi, K., Uda, S., Kudo, T., Komori, Y., Kubota, H., and Kuroda, S. (2013). The extraction of simple relationships in growth factor-specific multiple-input and multiple-output systems in cell-fate decisions by backward elimination PLS regression. PLoS One *8*, e72780.

Albeck, J.G., Mills, G.B., and Brugge, J.S. (2013). Frequency-modulated pulses of ERK activity transmit quantitative proliferation signals. Mol Cell *49*, 249–261.

Aoki, K., Kumagai, Y., Sakurai, A., Komatsu, N., Fujita, Y., Shionyu, C., and Matsuda, M. (2013). Stochastic ERK activation induced by noise and cell-to-cell propagation regulates cell density-dependent proliferation. Mol Cell *52*, 529–540.

Behar, M., and Hoffmann, A. (2010). Understanding the temporal codes of intra-cellular signals. Curr Opin Genet Dev *20*, 684–693.

Brightman, F.A., and Fell, D.A. (2000). Differential feedback regulation of the MAPK cascade underlies the quantitative differences in EGF and NGF signalling in PC12 cells. FEBS Lett *482*, 169–174.

Candès, E.J., and Fernandez-Granda, C. (2014). Towards a Mathematical Theory of Super-resolution. Commun Pure Appl Math *67*, 906–956.

Candès, E.J., and Recht, B. (2009). Exact Matrix Completion via Convex Optimization. Found Comput Math *9*, 717–772.

Candès, E.J., and Wakin, M.B. (2008). An Introduction To Compressive Sampling. IEEE Signal Proces Mag *25*, 21–30.

Candès, E.J., Wakin, M.B., and Boyd, S.P. (2008). Enhancing Sparsity by Reweighted ℓ1 Minimization. J Fourier Anal Appl *14*, 877–905.

Chung, J., Kubota, H., Ozaki, Y., Uda, S., and Kuroda, S. (2010). Timing-dependent actions of NGF required for cell differentiation. PLoS One *5*, e9011.

Donoho, D.L. (2006). Compressed sensing. IEEE Trans Inform Theory *52*, 1289–1306.

Doupé, D.P., and Perrimon, N. (2014). Visualizing and manipulating temporal signaling dynamics with fluorescence-based tools. Sci Signal *7*, re1.

Farah, C.A., and Sossin, W.S. (2012). The role of C2 domains in PKC signaling. In Calcium Signaling, M.S. Islam, ed. (Berlin: Springer), pp. 663–683.

Fazel, M. (2002). Matrix rank minimization with applications (PhD thesis, Stanford University).

Filippi, S., Barnes, C.P., Kirk, P.D., Kudo, T., Kunida, K., McMahon, S.S., Tsuchiya, T., Wada, T., Kuroda, S., and Stumpf, M.P. (2016). Robustness of MEK-ERK Dynamics and Origins of Cell-to-Cell Variability in MAPK signaling. Cell Rep *15*, 2524–2535.

Gerdin, M.J., and Eiden, L.E. (2007). Regulation of PC12 cell differentiation by cAMP signaling to ERK independent of PKA: Do all the connections add up? Science's STKE *2007*, pe15.

Gilmartin, A.G., Bleam, M.R., Groy, A., Moss, K.G., Minthorn, E.A., Kulkarni, S.G., Rominger, C.M., Erskine, S., Fisher, K.E., Yang, J., *et al.* (2011). GSK1120212 (JTP-74057) is an inhibitor of MEK activity and activation with favorable pharmacokinetic properties for sustained in vivo pathway inhibition. Clin Cancer Res *17*, 989–1000.

Gotoh, Y., Nishida, E., Yamashita, T., Hoshi, M., Kawakami, M., and Sakai, H. (1990). Microtubule-associated-protein (MAP) kinase activated by nerve growth factor and epidermal growth factor in PC12 cells. Eur J Biochem *193*, 661–669.

Hill, A.V. (1910). The possible effects of the aggregation of the molecules of haemoglobin on its dissociation curves. J Physiol (Lond) *40*, 4–7.

Janes, K.A., and Lauffenburger, D.A. (2006). A biological approach to computational models of proteomic networks. Curr Opin Chem Biol *10*, 73–80.

Janes, K.A., and Lauffenburger, D.A. (2013). Models of signalling networks - what cell biologists can gain from them and give to them. J Cell Sci *126*, 1913–1921.

Janes, K.A., and Yaffe, M.B. (2006). Data-driven modelling of signal-transduction networks. Nat Rev Mol Cell Biol *7*, 820–828.

Kholodenko, B., Yaffe, M.B., and Kolch, W. (2012). Computational approaches for

analyzing information flow in biological networks. Sci Signal *5*, re1.

Konishi, K., Uruma, K., Takahashi, T., and Furukawa, T. (2014). Iterative partial matrix shrinkage algorithm for matrix rank minimization. Signal Process *100*, 124–131.

Kudo, T., Uda, S., Tsuchiya, T., Wada, T., Karasawa, Y., Fujii, M., Saito, T.H., and Kuroda, S. (2016). Laguerre Filter Analysis with Partial Least Square Regression Reveals a Priming Effect of ERK and CREB on c-FOS Induction. PLoS One *11*, e0160548.

Liu, Z., Hansson, A., and Vandenberghe, L. (2013). Nuclear norm system identification with missing inputs and outputs. Syst & Control Lett *62*, 605–612.

Ljung, L. (1998). System Identification. In Signal Analysis and Prediction, A. Prochazka, N.G. Kingsbury, P.J.W. Payner, and J. Uhlir, eds. (New York: Springer), pp. 163–173.

Ljung, L. (2010). Perspectives on system identification. Ann Rev Control *34*, 1–12.

Lustig, M., Donoho, D.L., Santos, J.M., and Pauly, J.M. (2008). Compressed sensing MRI. IEEE Signal Process Mag *25*, 72–82.

Marshall, C. (1995). Specificity of receptor tyrosine kinase signaling: transient versus sustained extracellular signal-regulated kinase activation. Cell *80*, 179–185.

Nakakuki, T., Birtwistle, M.R., Saeki, Y., Yumoto, N., Ide, K., Nagashima, T., Brusch, L., Ogunnaike, B.A., Okada-Hatakeyama, M., and Kholodenko, B.N. (2010). Ligand-specific c-Fos expression emerges from the spatiotemporal control of ErbB network dynamics. Cell *141*, 884–896.

Ohashi, K., Komada, H., Uda, S., Kubota, H., Iwaki, T., Fukuzawa, H., Komori, Y., Fujii, M., Toyoshima, Y., Sakaguchi, K., *et al.* (2015). Glucose Homeostatic Law: Insulin Clearance Predicts the Progression of Glucose Intolerance in Humans. PLoS One *10*, e0143880.

Ongie, G., and Jacob, M. (2016). A fast algorithm for structured low-rank matrix recovery with applications to undersampled MRI reconstruction. Paper presented at: IEEE International Symposium on Biomedical Imaging (ISBI).

Ozaki, Y., Uda, S., Saito, T.H., Chung, J., Kubota, H., and Kuroda, S. (2010). A

quantitative image cytometry technique for time series or population analyses of signaling networks. PLoS One *5*, e9955.

Price, N.D., and Shmulevich, I. (2007). Biochemical and statistical network models for systems biology. Curr Opin Biotechnol *18*, 365–370.

Purvis, J.E., and Lahav, G. (2013). Encoding and decoding cellular information through signaling dynamics. Cell *152*, 945–956.

Qiu, M.-S., and Green, S.H. (1992). PC12 cell neuronal differentiation is associated with prolonged p21 ras activity and consequent prolonged ERK activity. Neuron *9*, 705–717.

Ravni, A., Bourgault, S., Lebon, A., Chan, P., Galas, L., Fournier, A., Vaudry, H., Gonzalez, B., Eiden, L.E., and Vaudry, D. (2006). The neurotrophic effects of PACAP in PC12 cells: control by multiple transduction pathways. J Neurochem *98*, 321–329.

Ryu, H., Chung, M., Dobrzynski, M., Fey, D., Blum, Y., Lee, S.S., Peter, M., Kholodenko, B.N., Jeon, N.L., and Pertz, O. (2015). Frequency modulation of ERK activation dynamics rewires cell fate. Mol Syst Biol *11*, 838.

Saito, T.H., Uda, S., Tsuchiya, T., Ozaki, Y., and Kuroda, S. (2013). Temporal decoding of MAP kinase and CREB phosphorylation by selective immediate early gene expression. PLoS One *8*, e57037.

Santos, S.D., Verveer, P.J., and Bastiaens, P.I. (2007). Growth factor-induced MAPK network topology shapes Erk response determining PC-12 cell fate. Nat Cell Biol *9*, 324–330.

Sasagawa, S., Ozaki, Y., Fujita, K., and Kuroda, S. (2005). Prediction and validation of the distinct dynamics of transient and sustained ERK activation. Nat Cell Biol *7*, 365–373.

Sumit, M., Takayama, S., and Linderman, J. (2017). New insights into mammalian signaling pathways using microfluidic pulsatile inputs and mathematical modeling. Integrative Biol *9*, 6–21.

Takahashi, T., Konishi, K., and Furukawa, T. (2012). Rank minimization approach to image inpainting using null space based alternating optimization. Paper presented at: 2012 19th IEEE International Conference on Image Processing (IEEE).

Takahashi, T., Konishi, K., Uruma, K., and Furukawa, T. (2016). Adaptive image

inpainting algorithm based on generalized principal component analysis. Paper presented at: Image, Video, and Multidimensional Signal Processing Workshop (IVMSP), 2016 IEEE 12th (IEEE).

Toettcher, J.E., Weiner, O.D., and Lim, W.A. (2013). Using optogenetics to interrogate the dynamic control of signal transmission by the Ras/Erk module. Cell *155*, 1422–1434.

Traverse, S., Gomez, N., Paterson, H., Marshall, C., and Cohen, P. (1992). Sustained activation of the mitogen-activated protein (MAP) kinase cascade may be required for differentiation of PC12 cells. Comparison of the effects of nerve growth factor and epidermal growth factor. Biochem J *288*, 351–355.

Uda, S., Saito, T.H., Kudo, T., Kokaji, T., Tsuchiya, T., Kubota, H., Komori, Y., Ozaki, Y., and Kuroda, S. (2013). Robustness and compensation of information transmission of signaling pathways. Science *341*, 558–561.

Vaudry, D., Stork, P., Lazarovici, P., and Eiden, L. (2002). Signaling pathways for PC12 cell differentiation: making the right connections. Science *296*, 1648–1649.

Watanabe, K., Akimoto, Y., Yugi, K., Uda, S., Chung, J., Nakamuta, S., Kaibuchi, K., and Kuroda, S. (2012). Latent process genes for cell differentiation are common decoders of neurite extension length. J Cell Sci *125*, 2198–2211.

Watanabe, M., Sowa, Y., Yogosawa, M., and Sakai, T. (2013). Novel MEK inhibitor trametinib and other retinoblastoma gene (RB)-reactivating agents enhance efficacy of 5-fluorouracil on human colon cancer cells. Cancer Sci *104*, 687–693.

Yamaguchi, T., Yoshida, T., Kurachi, R., Kakegawa, J., Hori, Y., Nanayama, T., Hayakawa, K., Abe, H., Takagi, K., Matsuzaki, Y., *et al.* (2007). Identification of JTP-70902, a p15(INK4b)-inductive compound, as a novel MEK1/2 inhibitor. Cancer Sci *98*, 1809–1816.

Yang, J., Wright, J., Huang, T.S., and Ma, Y. (2010). Image super-resolution via sparse representation. IEEE Trans Image Process *19*, 2861–2873.

Zechner, C., Seelig, G., Rullan, M., and Khammash, M. (2016). Molecular circuits for dynamic noise filtering. Proc Natl Acad Sci USA *113*, 4729–4734.

Zhang, K., Duan, L., Ong, Q., Lin, Z., Varman, P.M., Sung, K., and Cui, B. (2014).

Light-mediated kinetic control reveals the temporal effect of the Raf/MEK/ERK pathway in PC12 cell neurite outgrowth. PLoS One *9*, e92917.

8. Acknowledgements

I am full of gratitude to a lot of people who supported this study. I thank Prof. Shinya Kuroda so much for teaching principles of scientific research. This thesis is the result of the joint research of Dr. Masashi Fujii, Mr. Naoki Matsuda, Dr. Katsuyuki Kunida, Dr. Shinsuke Uda, Prof. Hiroyuki Kubota, Dr. Katsumi Konishi, Prof. Shinya Kuroda and the author. I received technically significant advice from Dr. Kosuke Umeda and Mr. Takamasa Kudo through frequent discussion. I thank Dr. Atsushi Hatano, Mr. Kaoru Ohashi, Dr. Takanori Sano, Mr. Toshiya Kokaji, Mr. Kentaro Kawata, Ms. Miharu Sato, Ms. Risa Kuribayashi and all the Kuroda laboratory members for their critical reading of this manuscript, helpful discussions, and technical assistance with the experiments. The computational analysis of this work was performed in part with support of the super computer system of the National Institute of Genetics (NIG), Research Organization of Information and Systems (ROIS).

In financial aspect, this work was supported by the Creation of Fundamental Technologies for Understanding and Control of Biosystem Dynamics, CREST, of the Japan Science and Technology Agency (JST)(#JPMJCR12W3), a Grant-in-Aid for Scientific Research on Innovative Areas (#17H06300, #17H06299), and a Grant-in-Aid for Japan Society for the Promotion of Science (JSPS) Research Fellow (#14J12344).

Finally, I deeply thank my family for her dedicated support.